Data in Brief 35 (2021) 106957

Contents lists available at ScienceDirect

Data in Brief

journal homepage: www.elsevier.com/locate/dib

Data Article

Data on the geology and structure of the Copper Cliff embayment and offset dyke, Sudbury Igneous Complex, Canada

Lucie Mathieu [a,*], Ulrich Riller [b], Lisa Gibson [c], Peter Lightfoot [d]

[a] Centre d'études sur les Ressources minérales (CERM), Département des Sciences appliquées (DSA), Université du Québec à Chicoutimi (UQAC), 555 boul. de l'université, Chicoutimi G7H 2B1 Quebec City, Canada
[b] Institut für Geologie, Universität Hamburg, Bundesstraße 55, 20146 Hamburg, Germany
[c] Vale, North American Exploration, 337 Power St., Copper Cliff Ontario, Canada
[d] Department of Earth Sciences, University of Western Ontario, 1151 Richmond Street N., London, Ontario N6A 5B7, Canada

ARTICLE INFO

Article history:
Received 22 February 2021
Revised 3 March 2021
Accepted 5 March 2021
Available online 16 March 2021

Keywords:
Sudbury Igneous Complex (SIC)
Copper Cliff Offset dyke (CCO)
Copper Cliff Embayment (CCE)
Magma
Fault reactivation
3D model
Structural restoration
Ni-Cu-PGE sulfide ore deposits

ABSTRACT

This contribution describes maps of the Copper Cliff Embayment (CCE) and Offset (CCO) dyke. The associated study attempts to unravel the mode of melt emplacement and the role of pre-impact faults in the deformation of the southern part of the Sudbury Igneous Complex (SIC). This contribution summarizes field observations (maps and images) and structural measurements. In addition, perspective views of the 3D Move model of the CCE and CCO dyke are provided. This data can be used by researchers and exploration geologists working in the Sudbury mining camp as a basis for future mapping, research and exploration efforts in the Copper Cliff area. This article is a co-submission to the following article: L. Mathieu, U. Riller, L. Gibson, P. Lightfoot (2021) Structural controls on the localization of the mineralized Copper Cliff embayment and the Copper Cliff offset dyke, Sudbury Igneous Complex, Canada, Ore Geol. Rev., https://doi.org/10.1016/j.oregeorev.2021.104071

DOI of original article: 10.1016/j.oregeorev.2021.104071
* Corresponding author.
E-mail address: lucie1.mathieu@uqac.ca (L. Mathieu).

https://doi.org/10.1016/j.dib.2021.106957

Specifications Table

Subject	Earth and Planetary Sciences, Geology, Economic Geology
Specific subject area	Structural geology and magma emplacement mechanism
Type of data	Table Figure
How data were acquired	Fieldwork was carried out during summers 2010 and 2011, west of the Sudbury city. The general geometry of the CCE and CCO dyke was modeled in 3D using the software Move (Midland Valley Ltd.).
Data format	Raw Analyzed
Parameters for data collection	Data for the 3D model correspond to surface mapping and 109 digitalized level plans of the Copper Cliff mine.
Description of data collection	Data were collected in the field using compass, notebook and hand-lens.
Data source location	Outcrops located west of the Sudbury city, in and south of the Copper Cliff town, Ontario, Canada.
Data accessibility	The data are available within this article.
Related research article	L. Mathieu, U. Riller, L. Gibson, P. Lightfoot (2021) Structural controls on the localization of the mineralized Copper Cliff embayment and the Copper Cliff offset dyke, Sudbury Igneous Complex, Canada, Ore Geol. Rev., https://doi.org/10.1016/j.oregeorev.2021.104071

Value of the Data

- The data document the geology and structure of outcrops exposed in the Copper Cliff area.
- The data provide a basis for additional and more detailed mapping in the study area.
- The data can be useful to exploration geologists interested in connecting underground faults and other geological features to surface exposure.
- The data can be used by any geologist interested in evaluating the mode of emplacement and structure of the CCE and CCO dyke.

1. Data Description

The Copper Cliff Embayment (CCE) outcrops north and south of the Clarabelle open pit (Fig. 1), Copper Cliff Mine, Copper Cliff town, Ontario, Canada. The main outcrops (Fig. 2) have been systematically documented as part of this study. Most outcrops correspond to inclusions-bearing rocks. The inclusions are small to large (Fig. 3a, b, c). The largest inclusions, or rafts, are most abundant along the margin of the CCE (Fig. 3d), while smaller inclusions are most abundant in the central part of the embayment (Fig. 3e). The shape-preferred orientation (SPO) of the inclusions is studied in plan view (Fig. 4a) to deduce trajectories of melt movements (Fig. 4b).

A large amount of structural data, including orientations of brittle-ductile fault planes (Figs. 5, 6, 7, 8, 9, 10 and Tables 1 to 4), brittle fault planes (Figs. 11, 12), and associated slicken lines (Fig. 11) were measured in the field. The main faults observed in and next to the CCE are the Lady Violet and the Pump Lake faults (Fig. 13). Folding in pre-impact rocks in contact with the CCE has also been studied (Fig. 14).

The Copper Cliff Offset (CCO) dyke has been mapped using five areas of excellent rock exposure (Fig. 15). These areas correspond to the following outcrops: 1) North Mine; 2) Copper Cliff town; 3) Copper Cliff hill; 4) South Mine; and 5) Southern outcrop. On the North Mine outcrop,

the CCO dyke intruded into the Creighton granite (Fig. 16) and transects foliation planes (Fig. 17). North of this outcrop, mingling of CCO material with Sudbury Breccia bodies can be observed (Figs. 18, 19). The rocks of the Copper Cliff town outcrop are strongly weathered (Fig. 20).

The Copper Cliff hill outcrop is located along a hiking trail (Fig. 21). This outcrop exposes the so-called quartz-diorite (QD) and inclusion-rich quartz diorite (IQD) phases of the CCO dyke, as well as contacts between CCO dyke and Sudbury Breccia bodies (Fig. 22), metasandstone of the McKim Formation (Fig. 23) and metavolcanic rocks of the Copper Cliff Formation (Fig. 24). The SPO of the inclusions was analyzed along the southern margin of the CCO dyke, where inclusions are most abundant (Figs. 25, 26). The inclusions are locally derived (Fig. 27). The orientation of fault and foliation planes were systematically measured in the field (Fig. 28).

The South Mine outcrop is located south of the railway to the Nickel refinery (Fig. 29). The contact between the CCO dyke and metagabbro is sharp and irregular (Fig. 30). Faults are most abundant along the contact between metagabbro and CCO dyke (Fig. 31). The CCO dyke contains metagabbro and sandstone inclusions (Fig. 32). On the Southern outcrop, the CCO dyke intruded into metasandstone of the Mississagi Formation (Fig. 33). The contact between the CCO dyke and metasandstone is sharp and irregular (Figs. 34).

Additional outcrops were visited to document the Creighton fault (Fig. 35), the 830 shear zone (Fig. 36), the Murray fault zone (Fig. 37) and the Evan fault (Fig. 38). Additional faults were studied underground (Fig. 39). The bulk of structural data measured in the field are reported in Tables 1 to 4 and are displayed using Rose diagrams, stereonet plots and Angelier plots (Fig. 40).

A simplified 3D Move model of the CCE and CCO dyke was produced using the software Move (Midland Valley Ltd.), surface mapping and digitalized level plans of the Copper Cliff mine (Fig. 41). Fault planes were simplified prior being integrated to the 3D model (Fig. 42). Perspective and plan views of the southern (Fig. 43), central (Fig. 44) and northern (Fig. 45) parts of the CCO dyke, as well as the CCE (Fig. 46) are available in this contribution. This 3D model was used to evaluate motion along the N°1-X and N°2-X fault planes (Fig. 47), as well as along the 900-OB, Evan, Creighton, F and G faults (Fig. 48).

Major lithological contacts, in footwall rocks, have also been integrated to the 3D Move model (Fig. 49). Using the model, we observed that the 830 structure (shear zone) is likely a ductile shear zone that induced folding in part of the CCO dyke (Fig. 50). The general geometrical characteristics of the CCO dyke were also documented using the 3D Move model (Fig. 51).

The 3D Move model was then restored along the 830 shear zone (Fig. 52), using the 3D Move software. Restoration along major faults followed (Fig. 53). Un-folding of the crater floor was then performed (Fig. 54). The CCE to CCO dyke contact, which may also have been folded, was also restored (Fig. 55).

The structural data measured in the field are reported by tables 1, 2, 3 and 4, which can be downloaded from the data repository Mendeley Data (see Data Availibility section below). Table 1 reports the orientation of brittle-ductile faults measured in the Copper Cliff Embayment (CCE). Table 2 reports the average orientation of the main faults that intersect the Copper Cliff Offset (CCO) dyke. Table 3 reports the orientation of the structures measured in the Copper Cliff Offset (CCO) dyke and its hosting rocks. Table 4 reports the averaged orientation and motion of the major faults.

2. Experimental Design, Materials and Methods

This study relies on detailed mapping of the CCE and CCO dyke performed during summers 2010 and 2011. The studied SIC rocks contain a large amount of xenoliths that can also be referred to as inclusions. The shape-preferred orientation (SPO) of the inclusions is studied in plan view following the method delineated by Launeau and Robin [3]. A large amount of structural data, including orientations of quartz veins, fault planes (brittle and brittle-ductile faults) and associated slicken lines were measured in the field. Structural data are presented using strike and trend values restricted between azimuths of 000° and 180°. The percentage of dip-slip is calculated for each fault using the pitch angle. The kinematics of the faults is expressed as fol-

lows: 1) an oblique-slip fault that has accommodated reverse and dextral strike-slip movement is referred to as a dextral-reverse oblique-slip fault; and 2) faults that have accommodated >80% and <30% of dip-slip movement are referred to, respectively, as reverse and strike-slip faults.

To comment on the general geometry of the CCE and CCO dyke, a simplified 3D model was produced using the software Move (Midland Valley Ltd.). This 3D model is constrained by surface mapping, as well as 109 digitalized level plans of the Copper Cliff mine. Where the CCO dyke has not been mapped, the Datamine 3D model of the partner company, Vale, was used to fill the gaps. The maps located <100 vertical feet from each other were then combined to produce 19 simplified level plans. These plans were then digitized as curves using the software 2D-Move and the curves were turned into surfaces using the software 3D-Move.

The 3D Move model comprises simplified surfaces that represent the CCO dyke, the CCE, a part of the crater floor, the main lithological contacts observed in footwall rocks, as well as the major faults that intersect the studied intrusion. These surfaces extend from present erosion surface to the 4000 level (from the 250 m to the -970 m elevations). The (x, y, z) data of the 3D Move model are expressed in feet, using the company coordinate system of the Copper Cliff mine. The 3D Move model was then restored sequentially, assuming that brittle deformation postdates ductile deformation; i.e., 'un-faulting' was performed before 'un-folding' in the software. The translation tools of the 3D-Move software attributes new (x, y, z) coordinates to each node of a surface without changing its shape. This tool was used to 'un-fault' the model using the mean total slip estimated for each fault. 'Un-folding' was then performed using fold axes deduced from the general morphology of the CCE and CCO dyke.

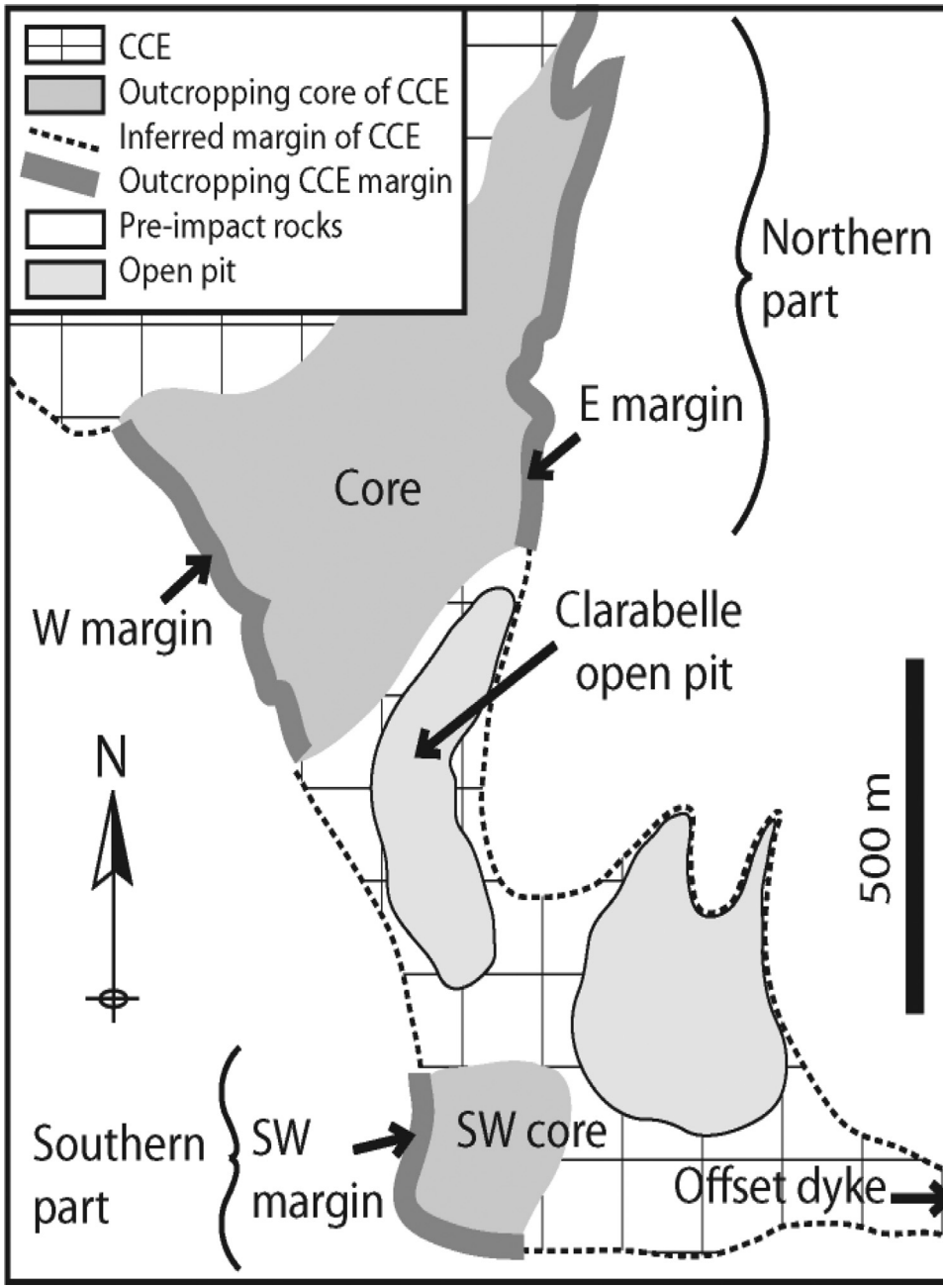

Fig. 1. General map of the CCE.

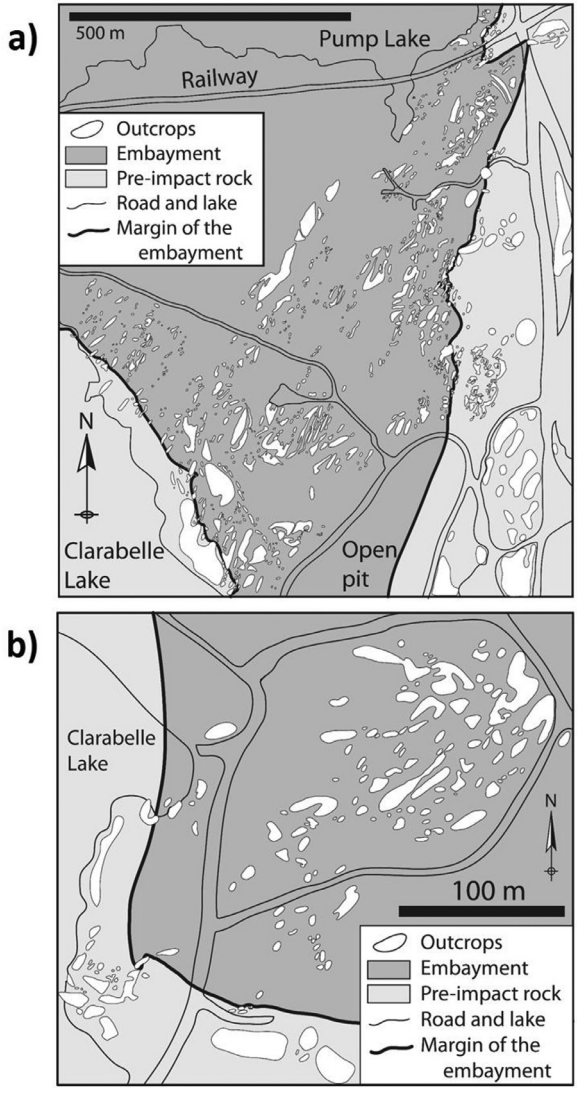

Fig. 2. Map displaying the outcrops visited in the field in the northern (a) and southern (b) parts of the CCE (see Fig. 1 for location).

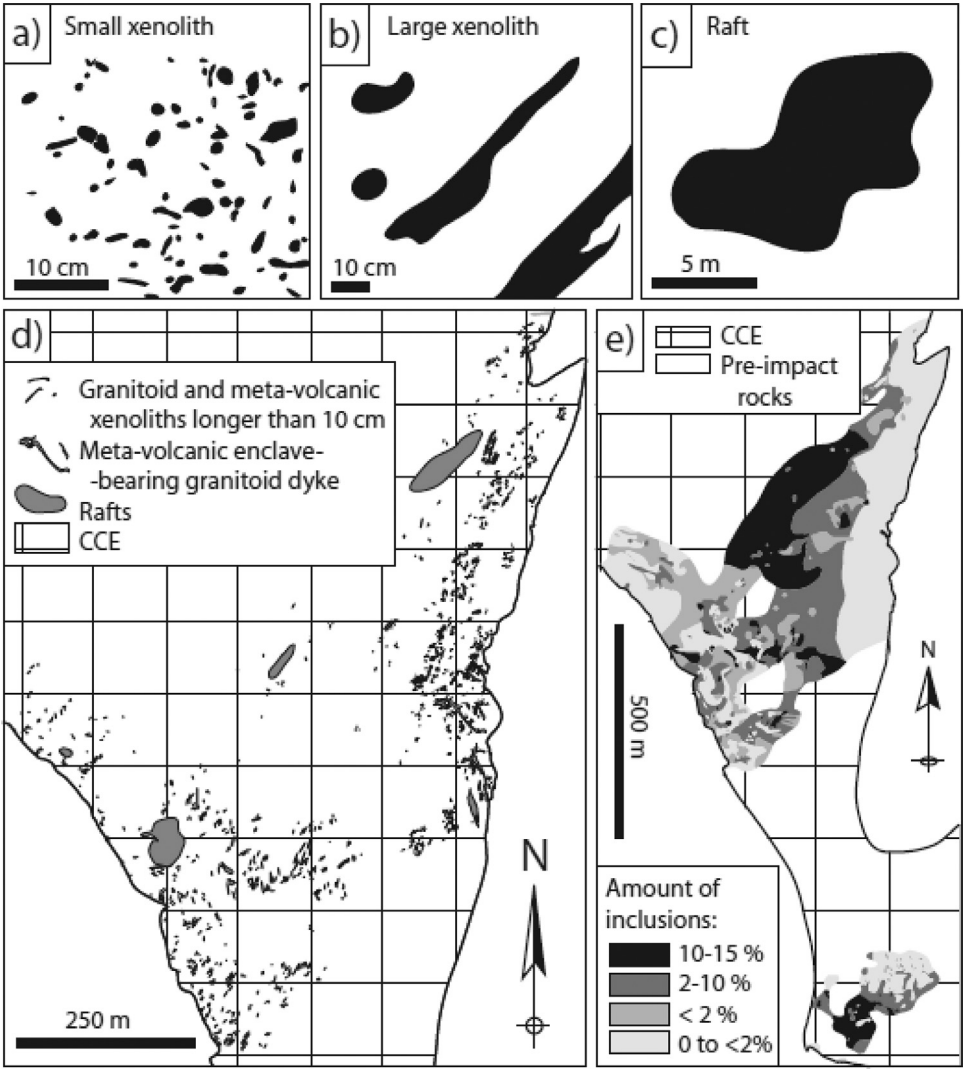

Fig. 3. a-c) Sketches of small xenoliths (a), large xenoliths (b) and rafts (c); d) Map displaying the distribution of rafts and large xenoliths in the northern part of the CCE; e) Map showing the distribution of small xenoliths in the CCE.

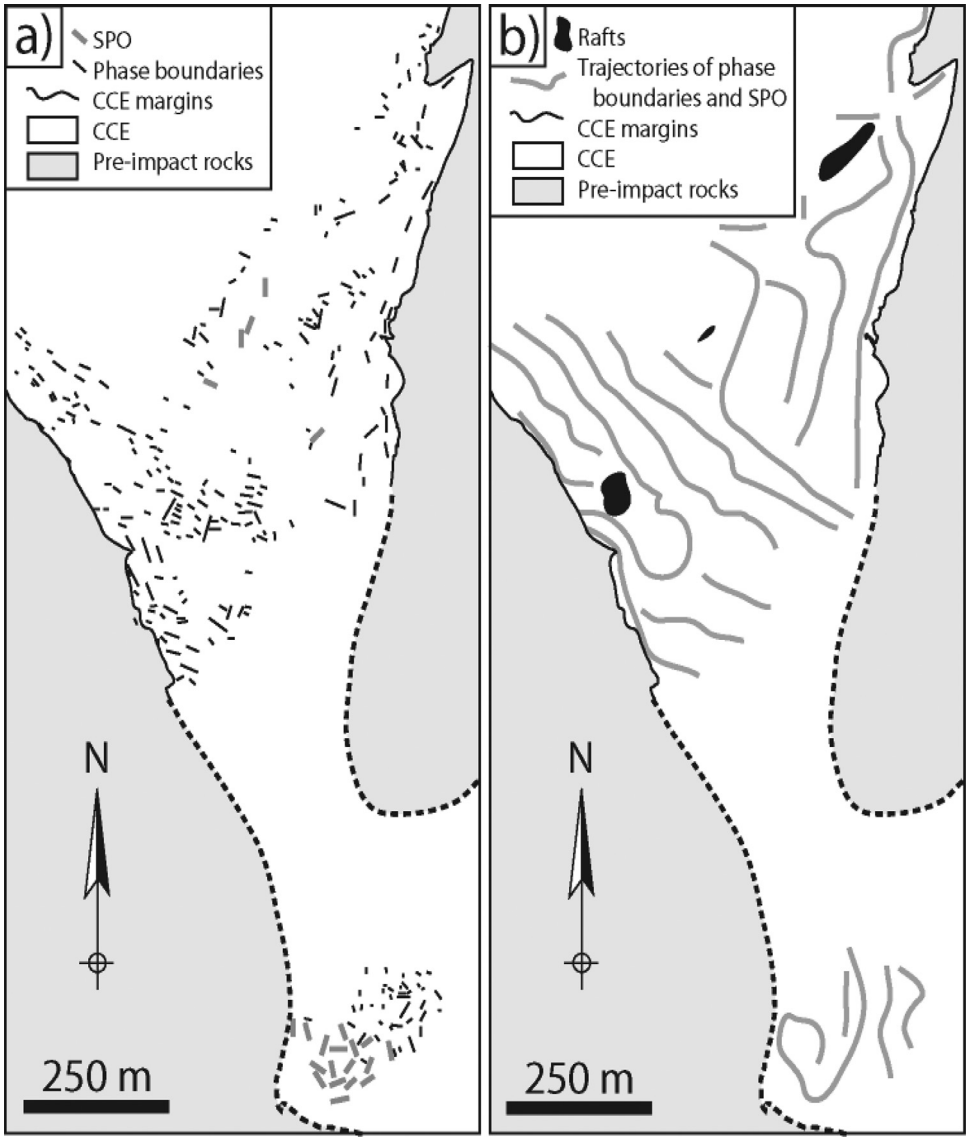

Fig. 4. Maps displaying the linear fabrics of the CCE; a) Map displaying SPO (shape-preferred orientation) results and phase boundaries; b) Map displaying hand-drawn trajectories of SPO and phase boundaries.

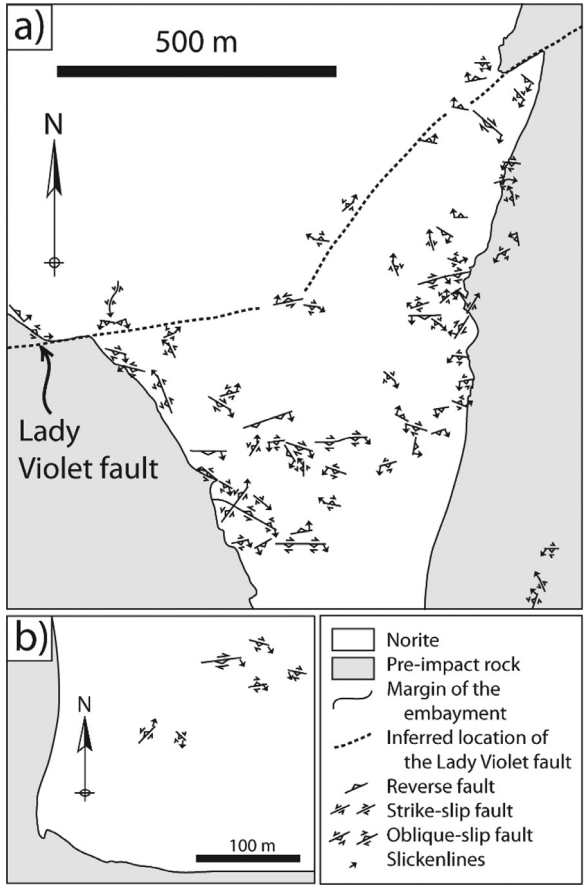

Fig. 5. Map displaying the brittle-ductile faults of the CCE.

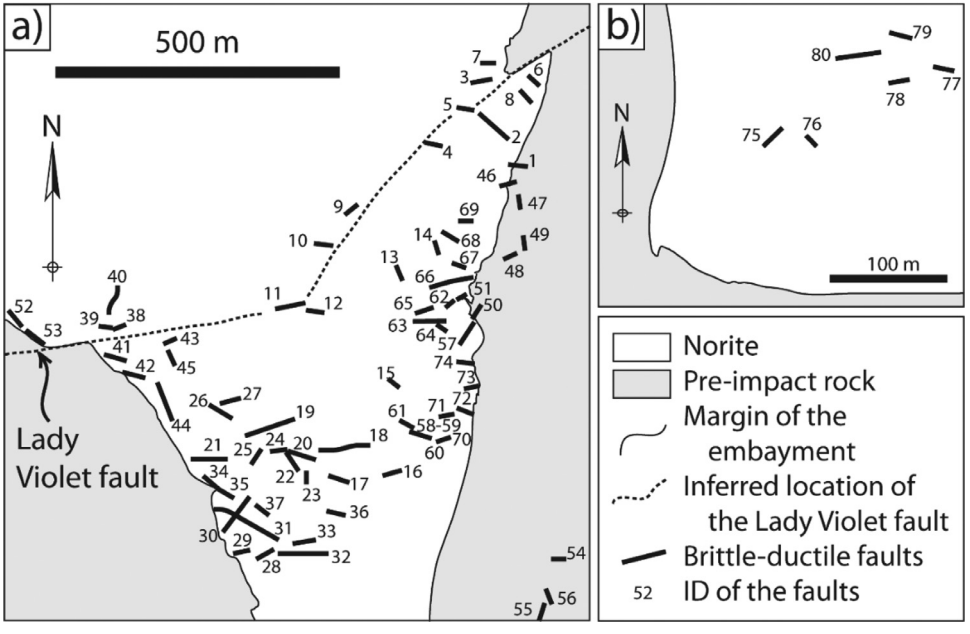

Fig. 6. Map displaying the ID of the brittle-ductile faults of the CCE.

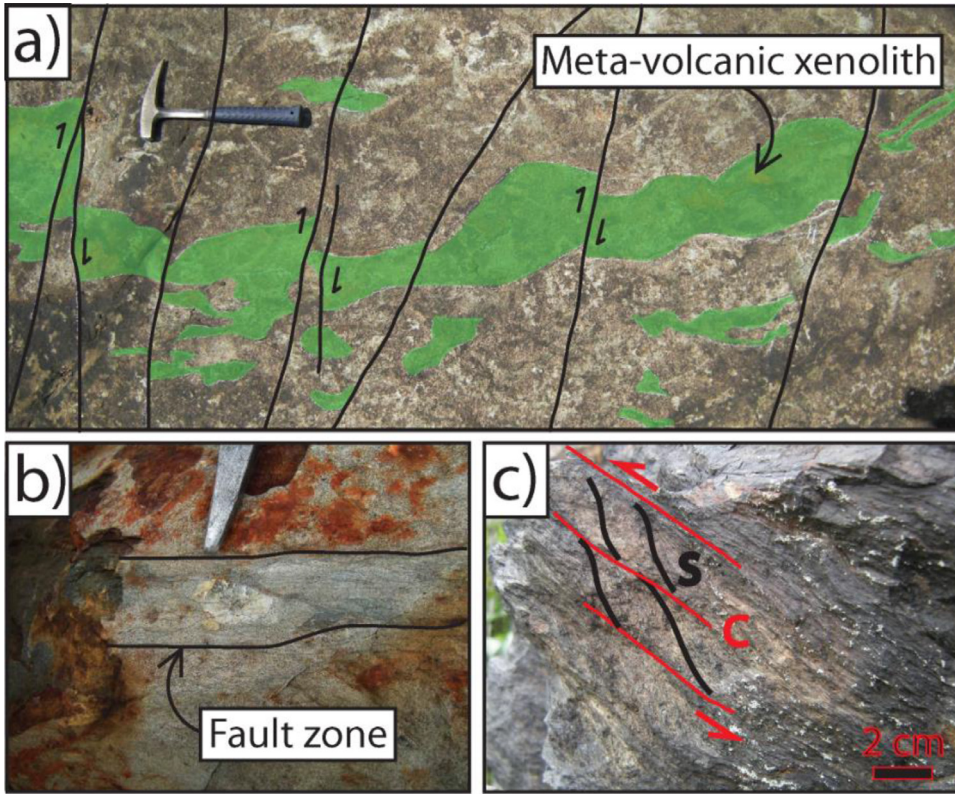

Fig. 7. Outcrop photographs of brittle faults (a), of a brittle-ductile fault (b) and of the Lady Violet fault plane (c).

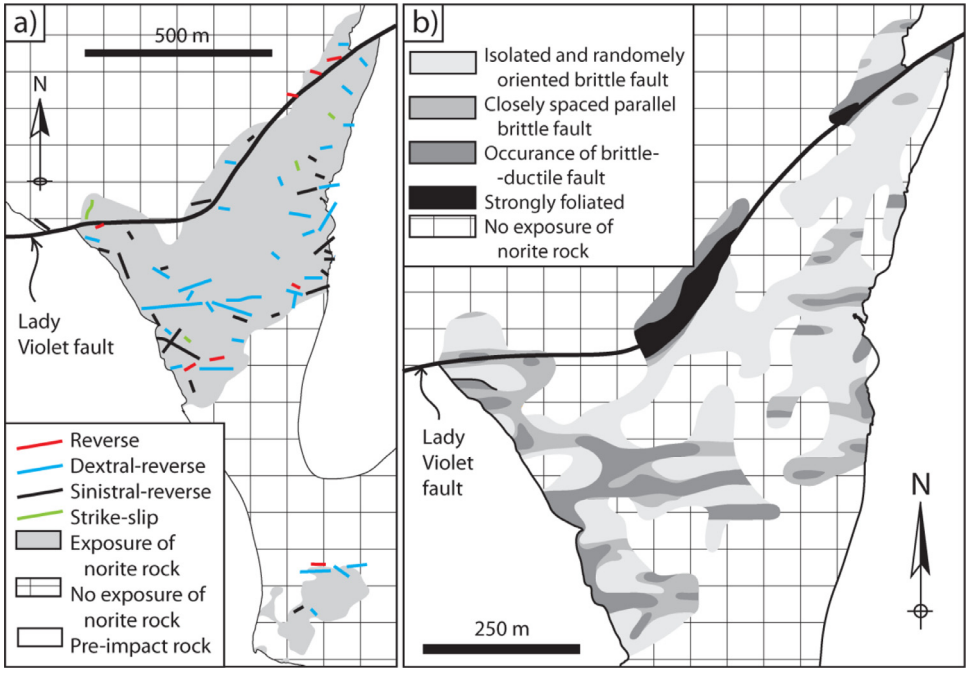

Fig. 8. a) Map displaying the distribution of brittle-ductile faults in the CCE; b) Strain intensity map of the northern part of the CCE.

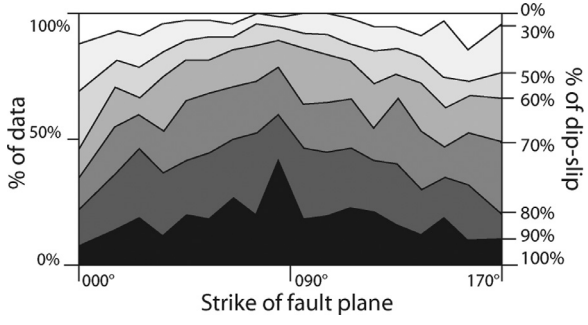

Fig. 9. Histogram plot of the kinematics of brittle faults expressed in percentage of dip-slip versus the strike of fault planes.

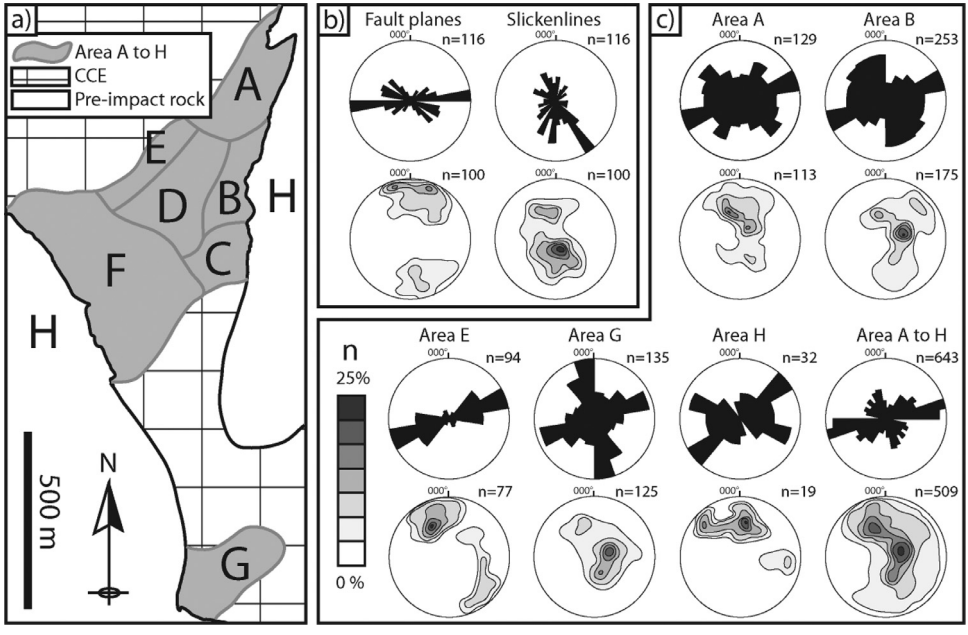

Fig. 10. Structural field data; a) Map of the CCE locating areas A to H; b-c) Rose diagrams and contour plots of the strike, trend and dip of the brittle-ductile fault planes and slickenlines (b) and of the quartz veins (c).

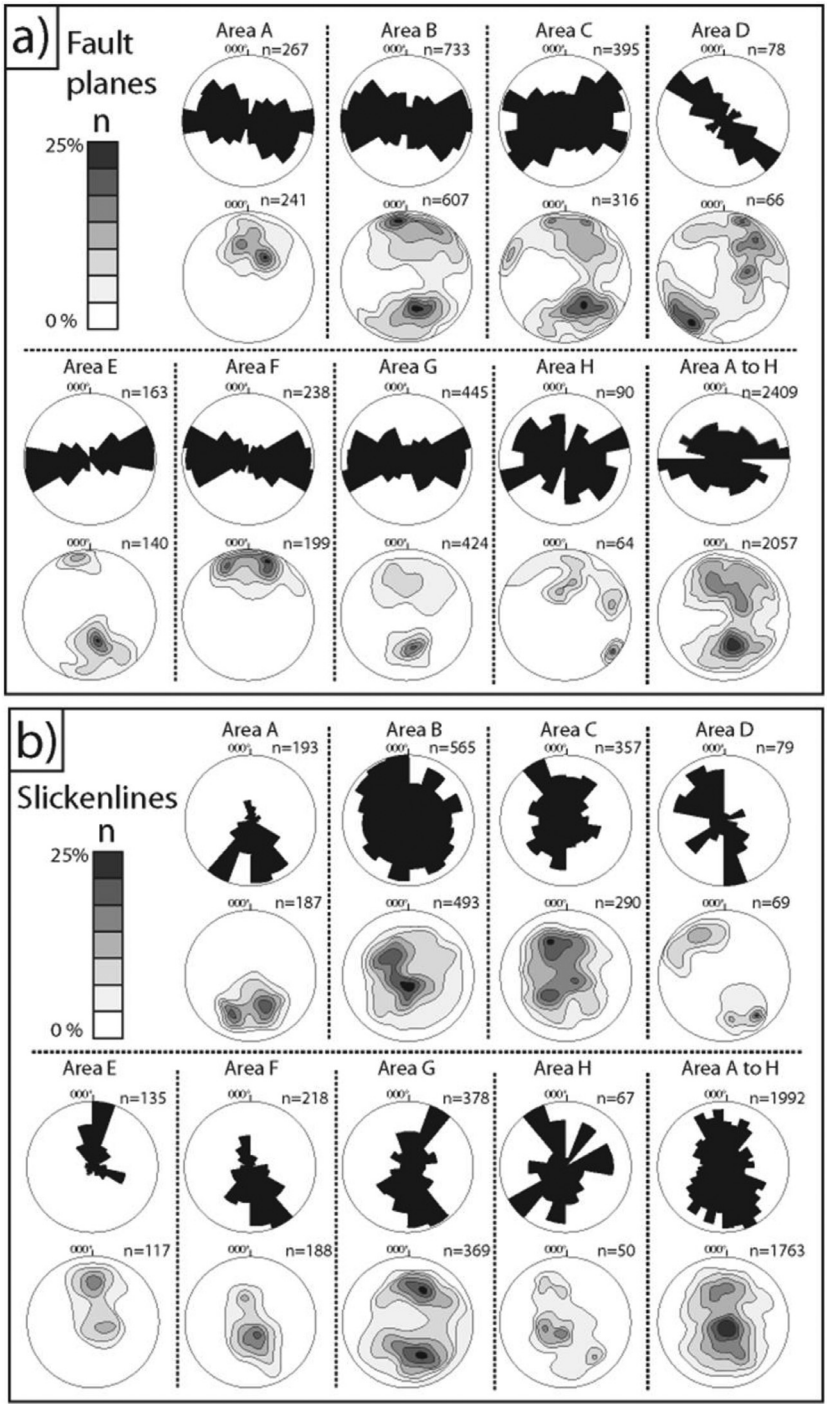

Fig. 11. Rose diagrams and contour plots of the orientation of the brittle fault planes.

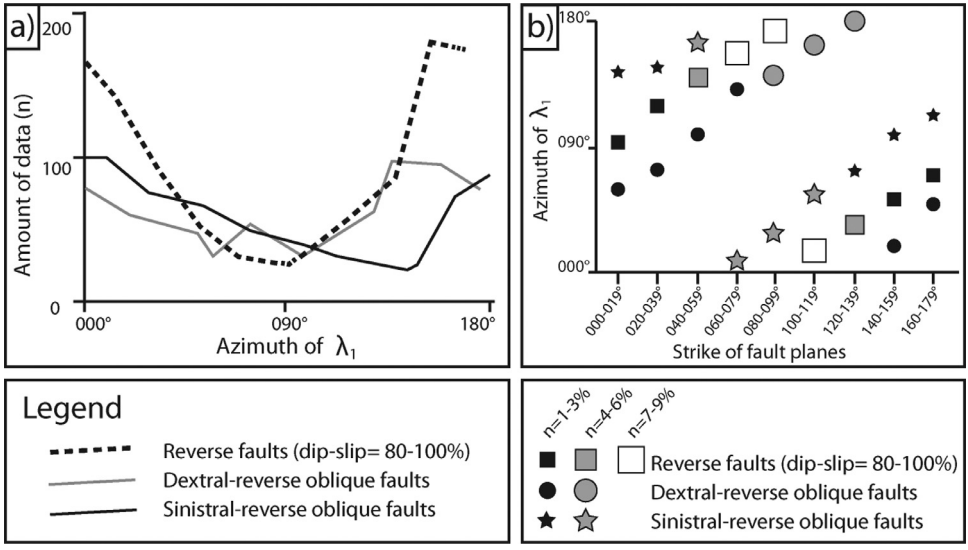

Fig. 12. Results of the fault slip data analysis carried on the brittle faults; a) Plot of the orientation of λ_1 versus the amount of data (n); b) Plot of the strike of brittle fault planes versus λ_1 trends.

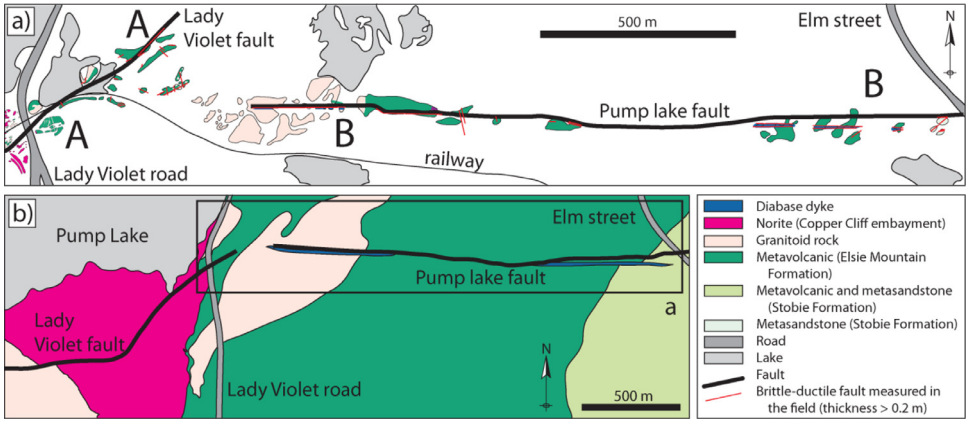

Fig. 13. Geological maps displaying the Lady Violet and Pump Lake faults; a) Map displaying the Pump Lake fault and the outcrops visited in the field; b) Map of the CCE and pre-impact rocks (after [1]).

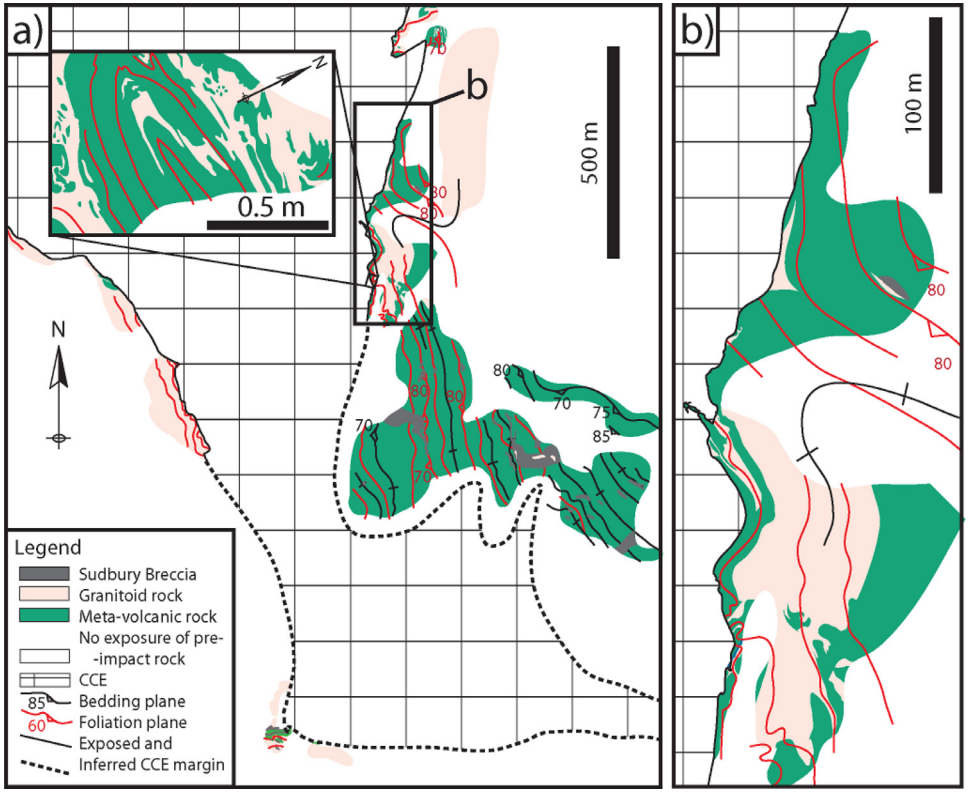

Fig. 14. Geological map of the pre-impact rocks that are in contact with the CCE.

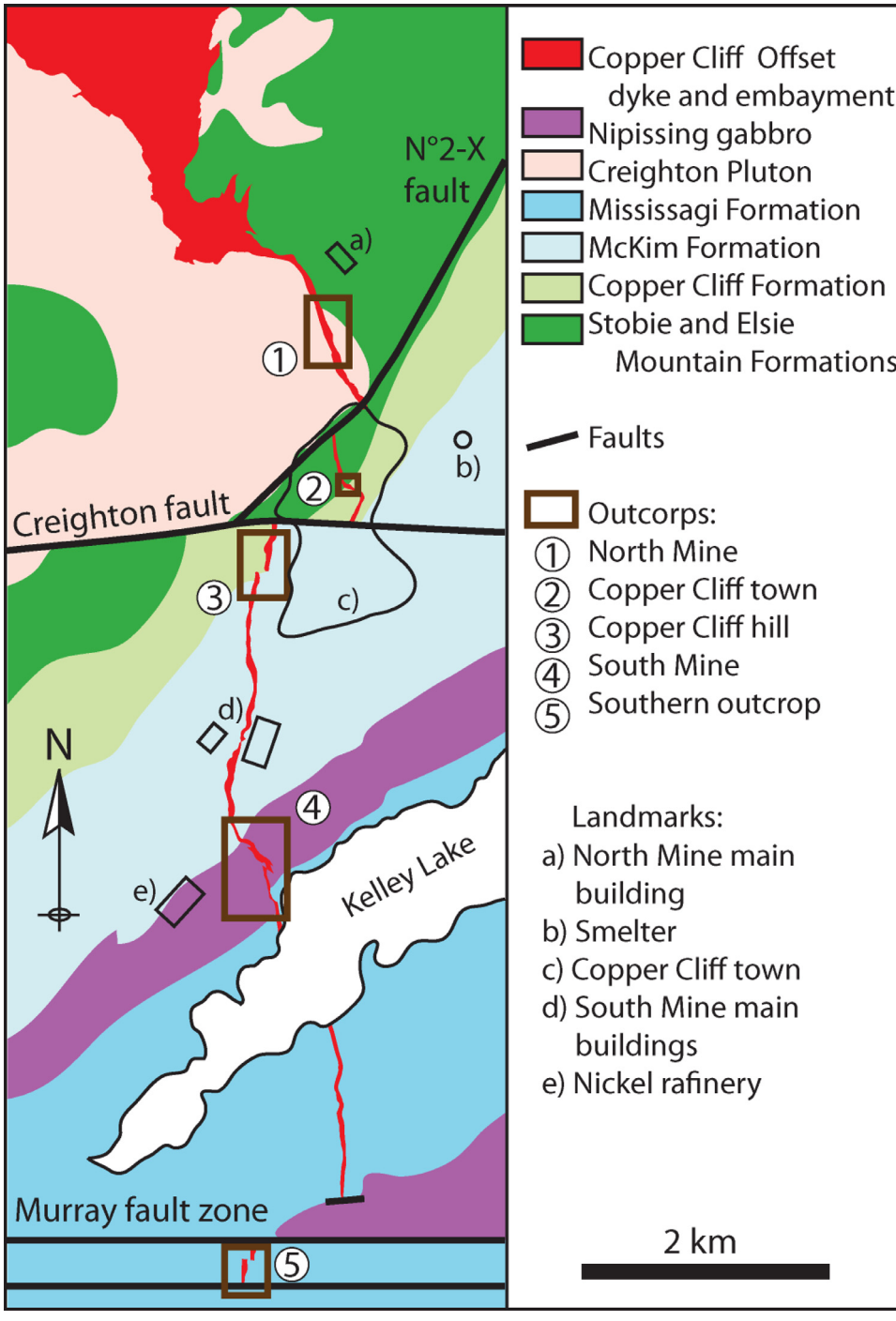

Fig. 15. Geological map of the CCO dyke and pre-impact rocks (geology is after [1]).

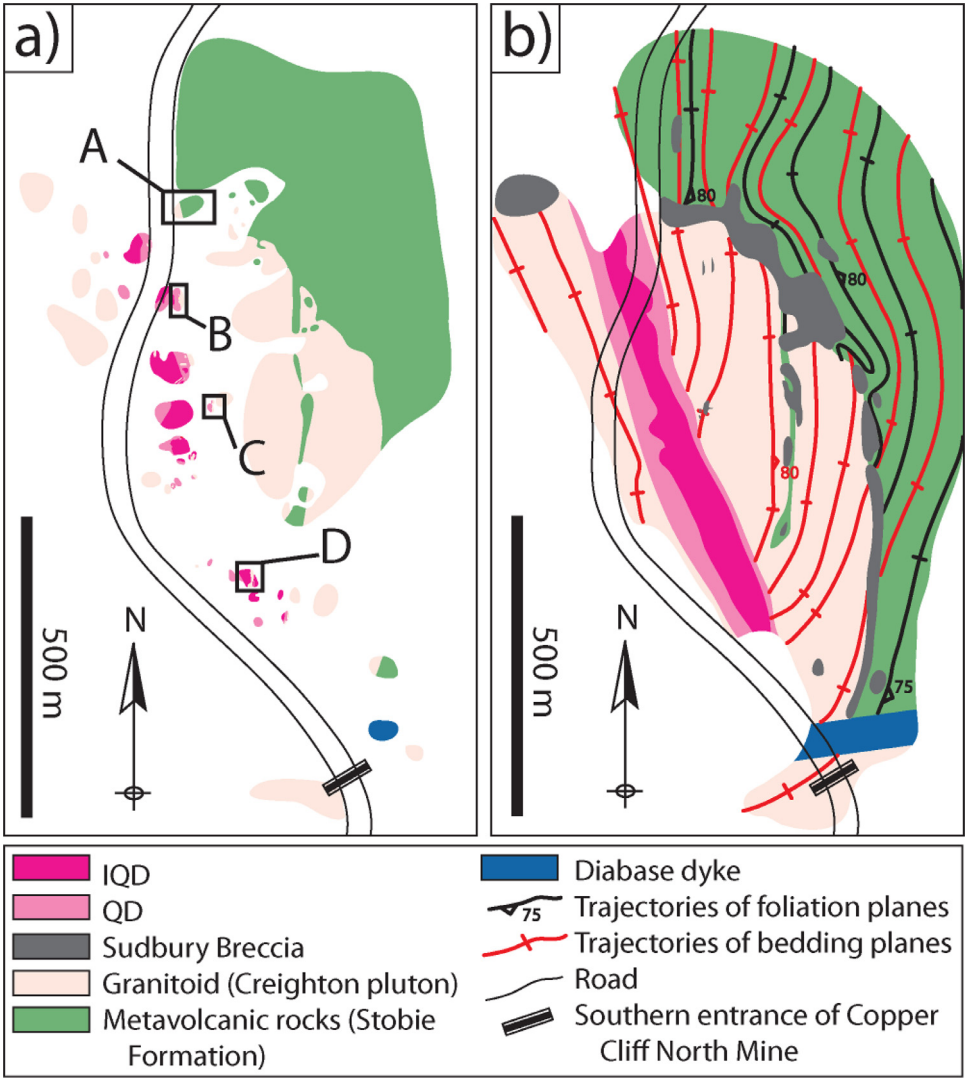

Fig. 16. Geological map of the North Mine outcrop; a) Map displaying the outcrops visited in the field; b) Geological map of the CCO dyke and surrounding pre-impact rocks. See Fig. 17 for detailed maps of areas B, C and D, and Fig. 18 for detailed map of area A.

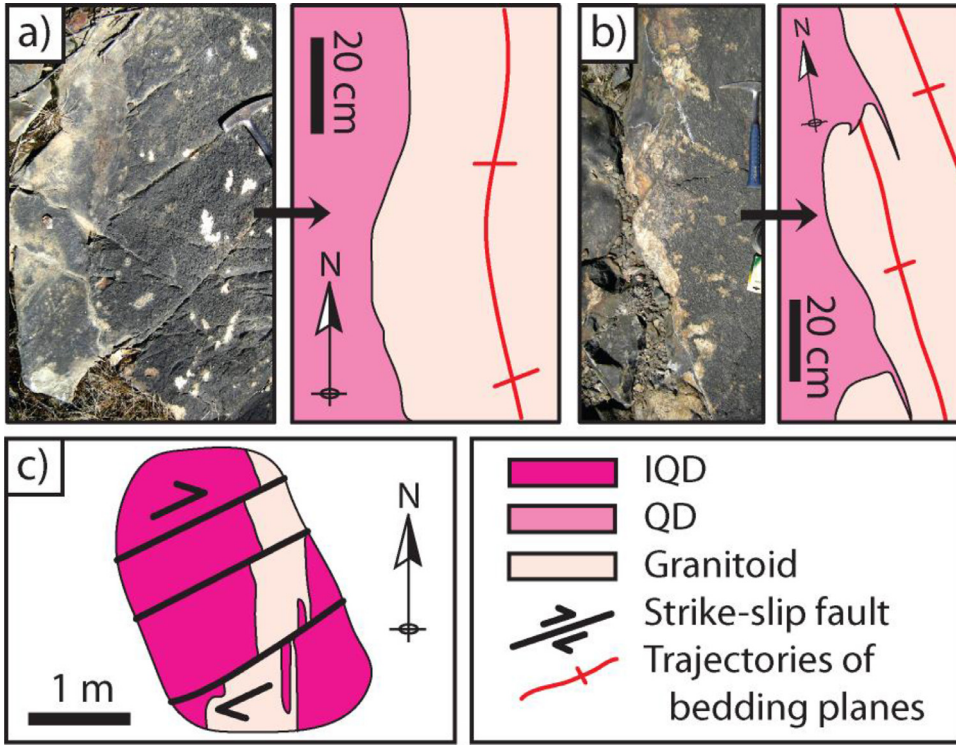

Fig. 17. Detailed maps of the CCO dyke; a-b) Outcrop photographs and sketches of the contact between QD and granitoid rocks (area B and C); c) Detailed map of a 4 m long granitoid xenolith (area D). See Fig. 16 for location.

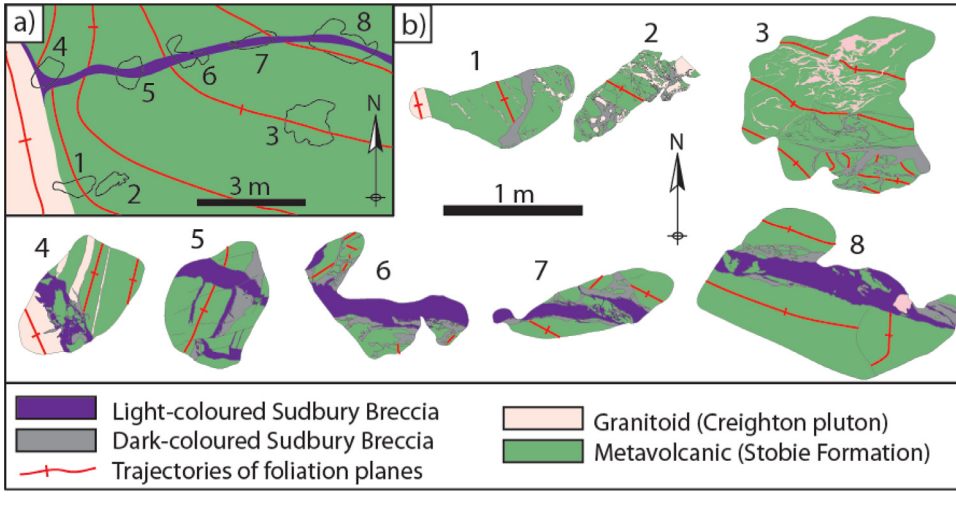

Fig. 18. Detailed map of Sudbury Breccia outcrops; a) Geological map of the study area (area A on Fig. 16); b) Detailed map of outcrops visited in the field and located on map (a).

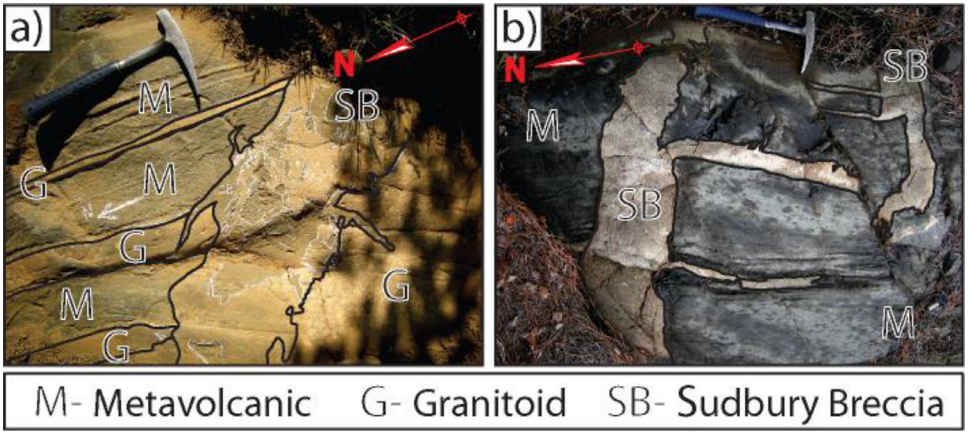

Fig. 19. Field photographs of the outcrops displayed in Fig. 18; a) Outcrop N°4; b) Outcrop N°5.

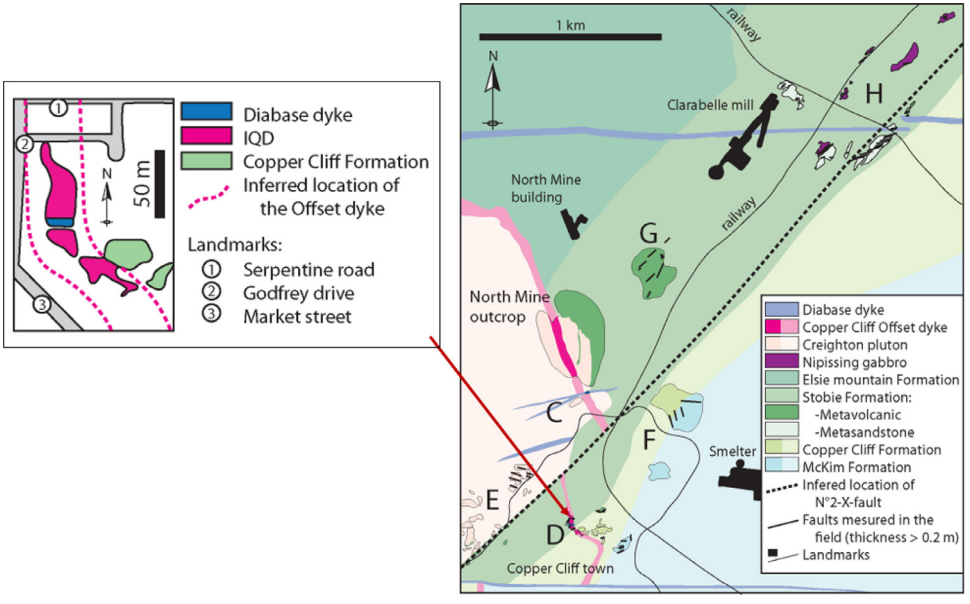

Fig. 20. Simplified geological map (after [1]) of the North Mine and Copper Cliff town outcrops.

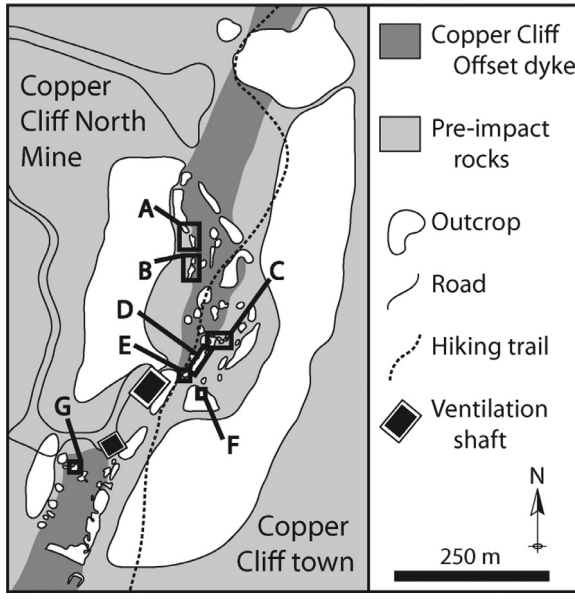

Fig. 21. Map displaying the outcrops visited in the field (Copper Cliff hill outcrop). For detailed geological map, please refer to companion article.

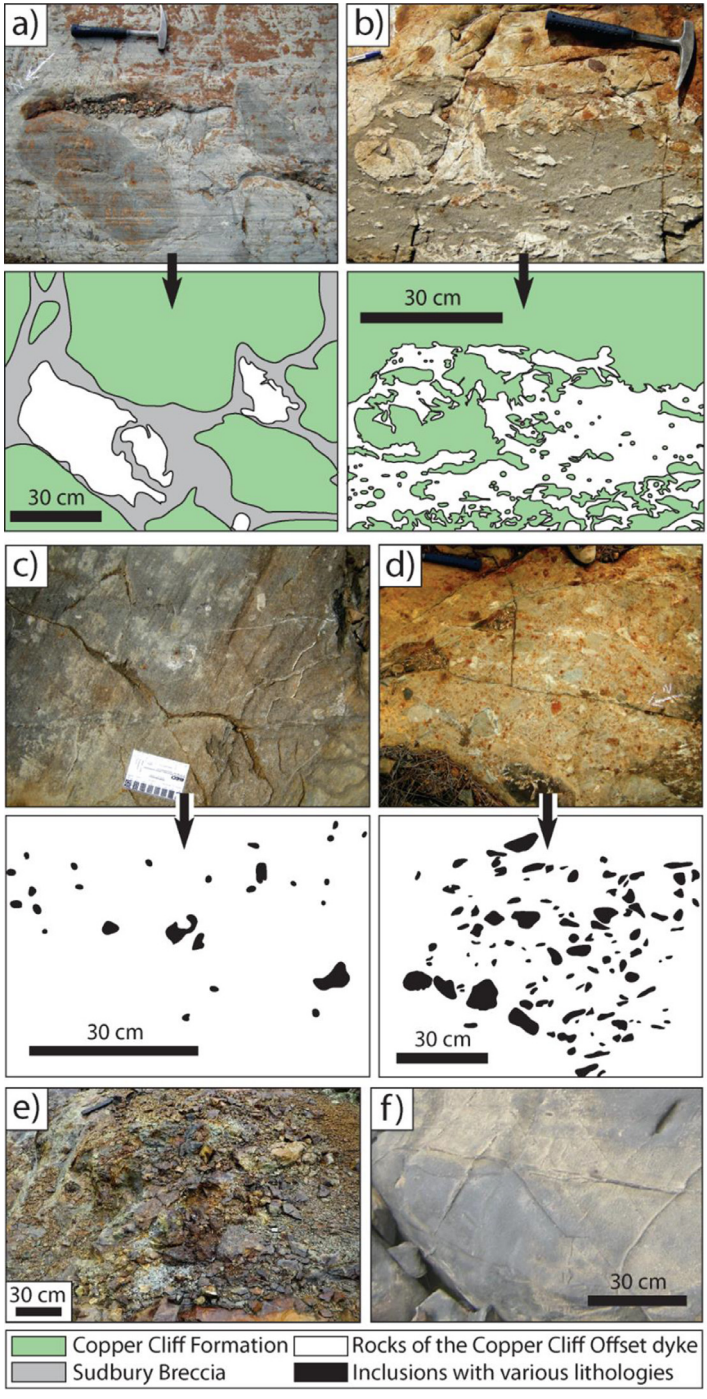

Fig. 22. Outcrop photographs and sketches; a) Thin-grained QD bulbs located in the matrix of Sudbury Breccia bodies (area F on Fig. 21); b) Contact relationship between QD rocks and the Copper Cliff Formation (area B on Fig. 21).
Fig. 22 (suite): Outcrop photographs and sketches: c) Sulfide bearing IQD rock; d) Inclusion-rich IQD rock; e) Sulfide-rich IQD rock; f) QD rock.

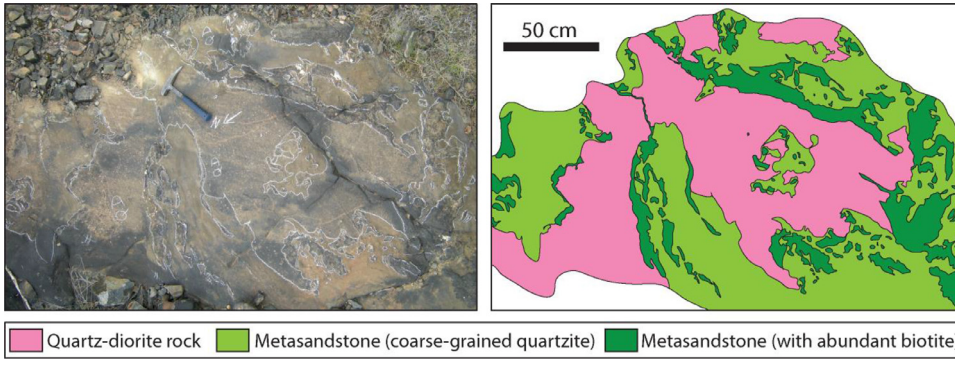

Fig. 23. Outcrop photograph and sketch of a meta-sandstone inclusion located in QD (area G on Fig. 21).

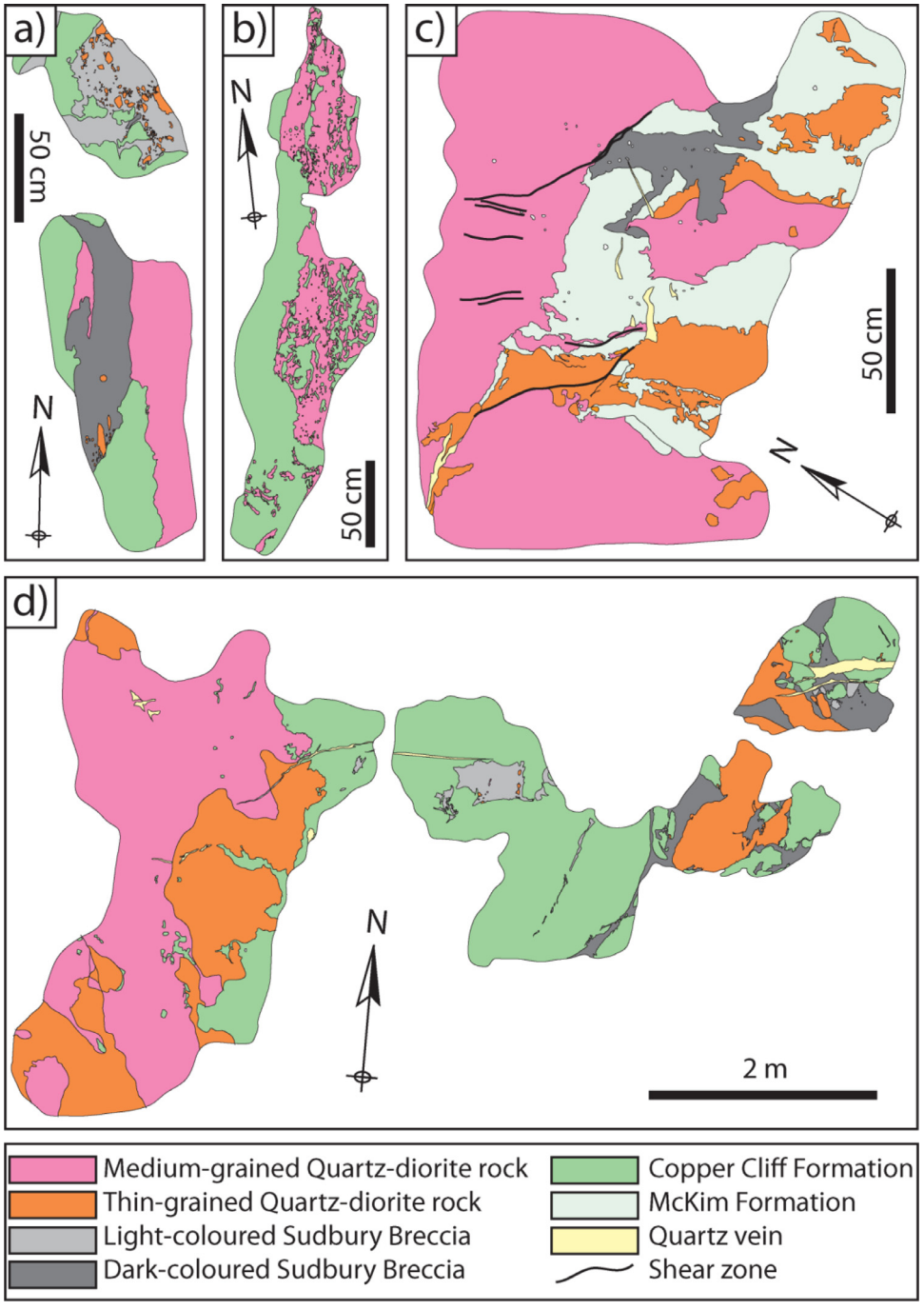

Fig. 24. Detailed maps of the margin of the CCO; a) Map of the contact between the CCO, the Copper Cliff Formation and Sudbury Breccia (area A on Fig. 21); b) Map of the contact between the CCO and the Copper Cliff Formation (area B on Fig. 21); c) Map of the contact between the CCO and the McKim Formation (area E of Fig. 21); d) Map of the contact between the CCO, the Copper Cliff Formation and Sudbury Breccia (area C of Fig. 21).

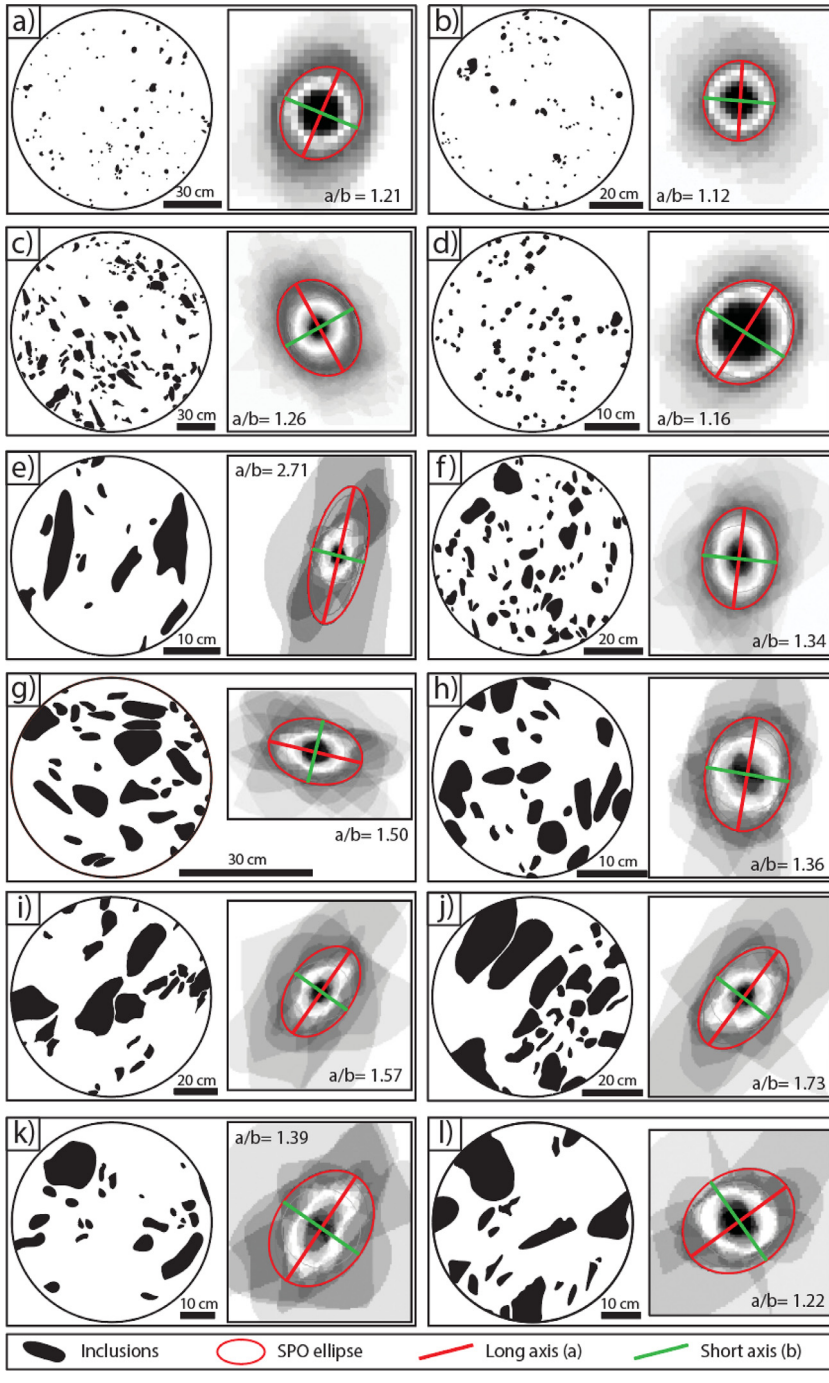

Fig. 25. Inclusions drawn from outcrop photographs and results of the SPO analysis presented by SPO ellipses (see Fig. 26 for a location of areas a to l).

Fig. 25 (suite): Inclusions drawn from outcrop photographs and results of the SPO analysis presented by SPO ellipses (see Fig. 26 for a location of areas a to l).

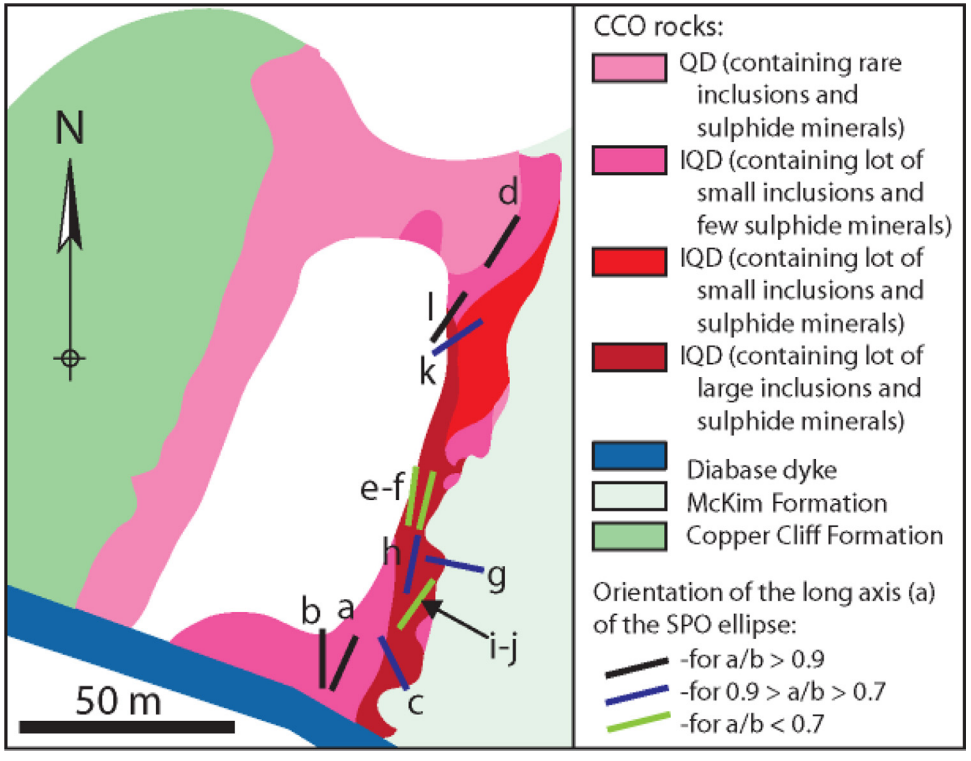

Fig. 26. Map of the southern part of the Copper Cliff hill outcrop displaying the results of the SPO analysis carried in areas a to l.

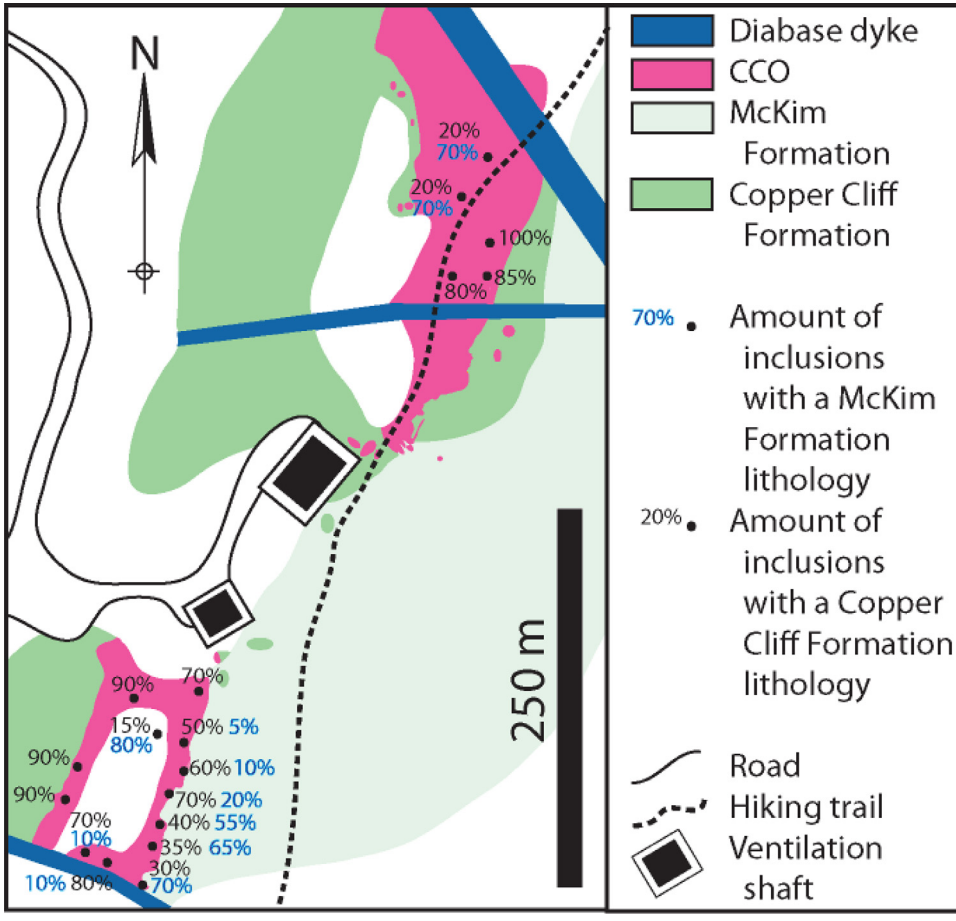

Fig. 27. Map displaying the distribution of the metasandstone and felsic metavolcanic inclusions in the CCO dyke (Copper Cliff hill outcrop).

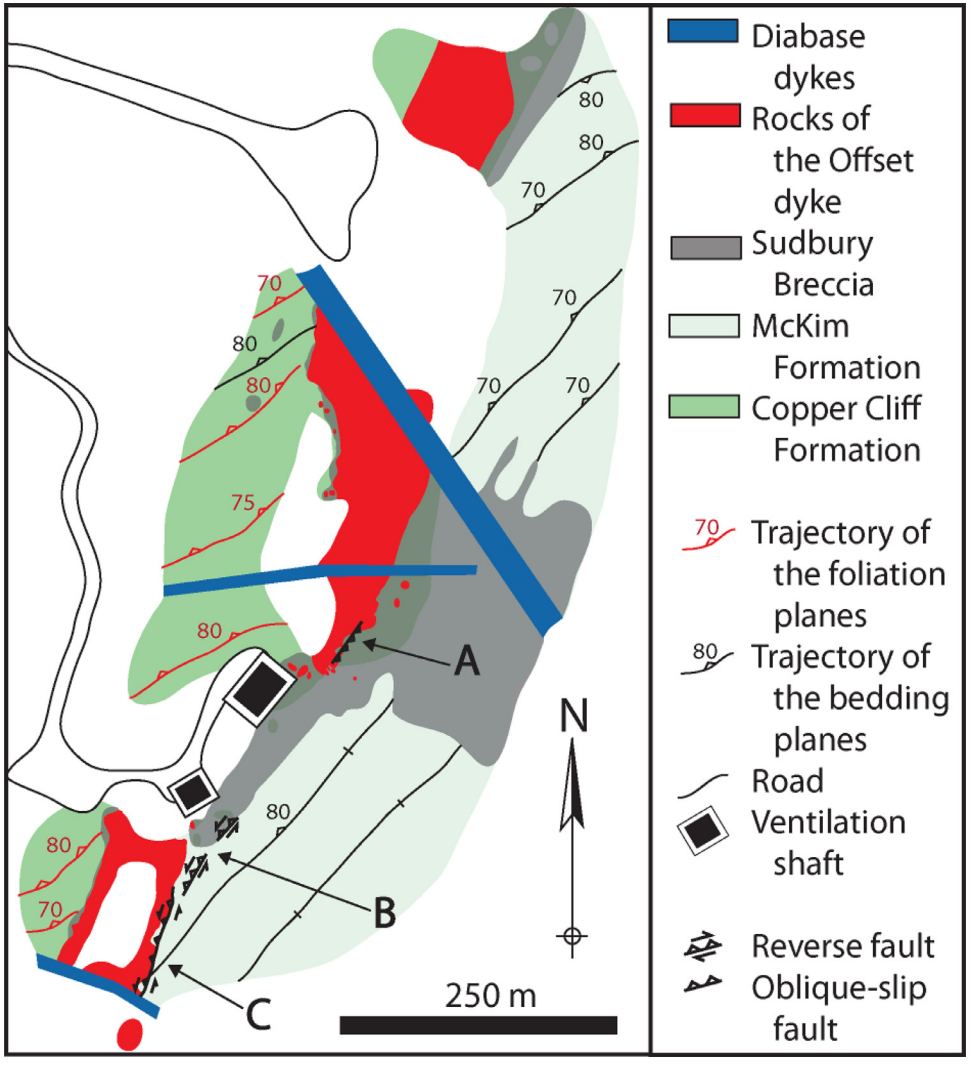

Fig. 28. Structural map of the Copper Cliff hill outcrop.

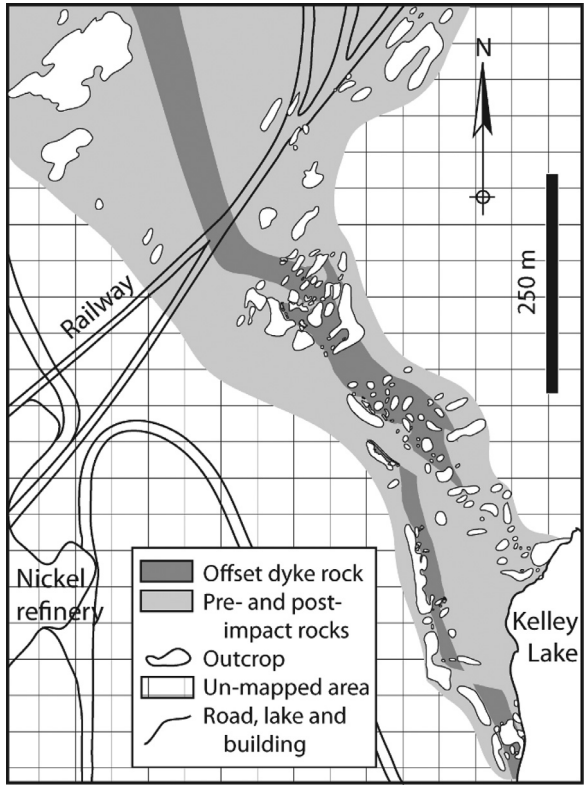

Fig. 29. Map displaying the outcrops of the South Mine area. Please refer to co-submitted article for a geological map of the South Mine outcrop.

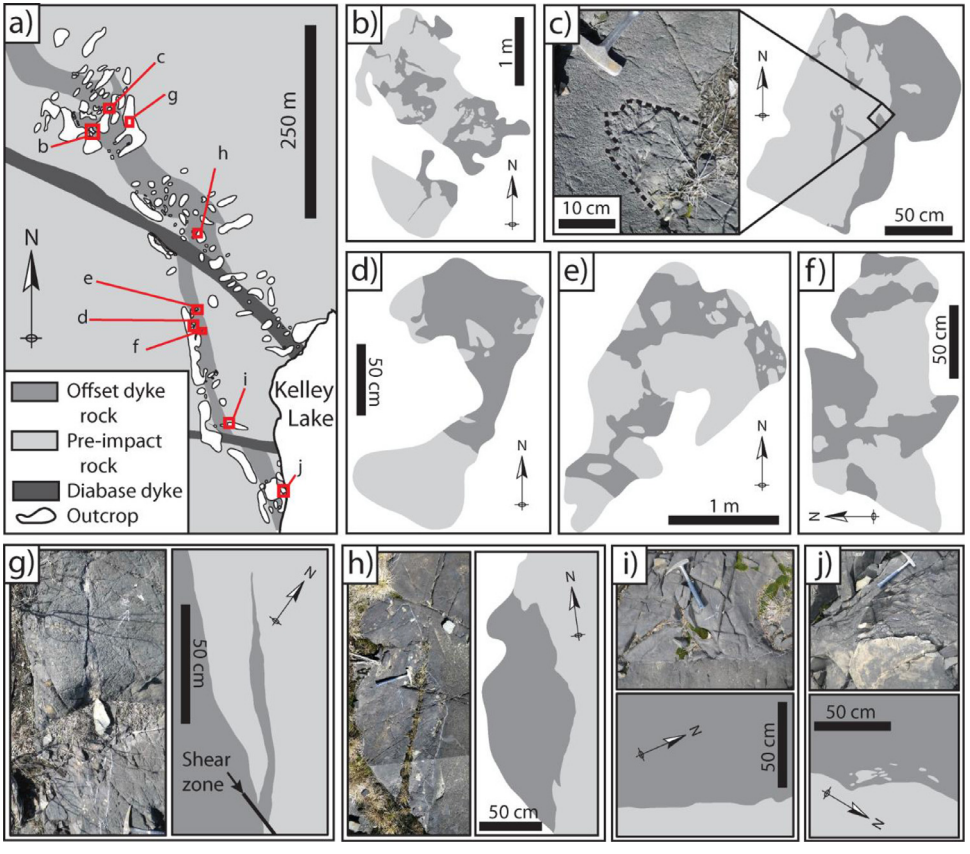

Fig. 30. Outcrop photographs and sketches of the margin of the CCO dyke displaying the contact relationship between the CCO dyke and metagabbro (pre-impact rocks).

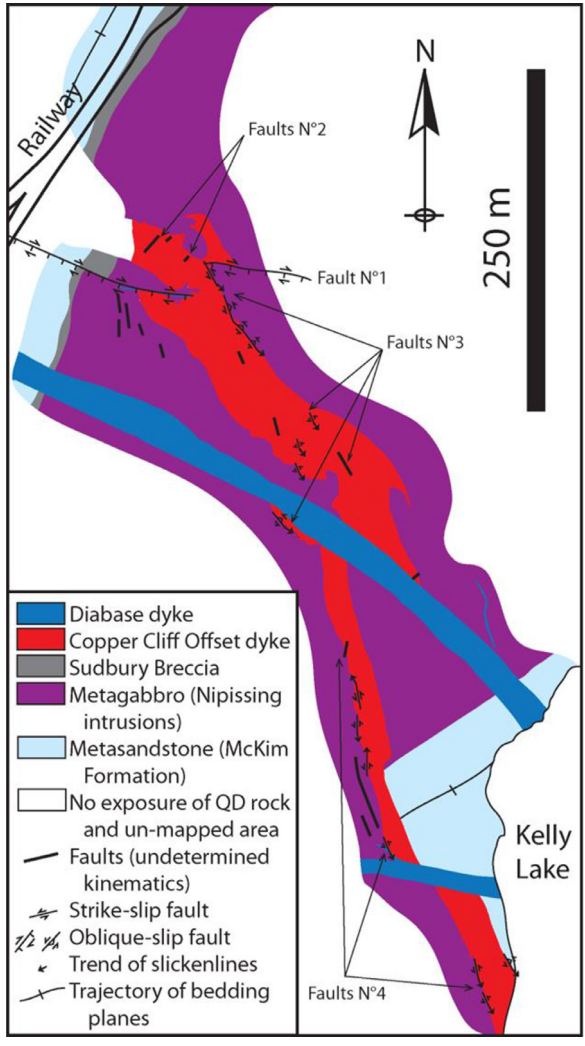

Fig. 31. Structural map of the South Mine outcrop.

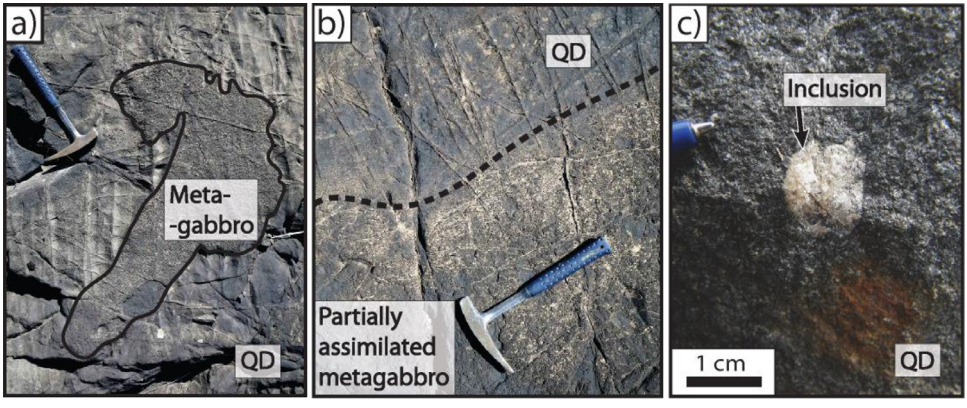

Fig. 32. Outcrop photographs of CCO rocks; a) Metagabbro xenolith in QD; b) Partially assimilated metagabbro xenolith in QD; c) Metasandstone inclusions in IQD.

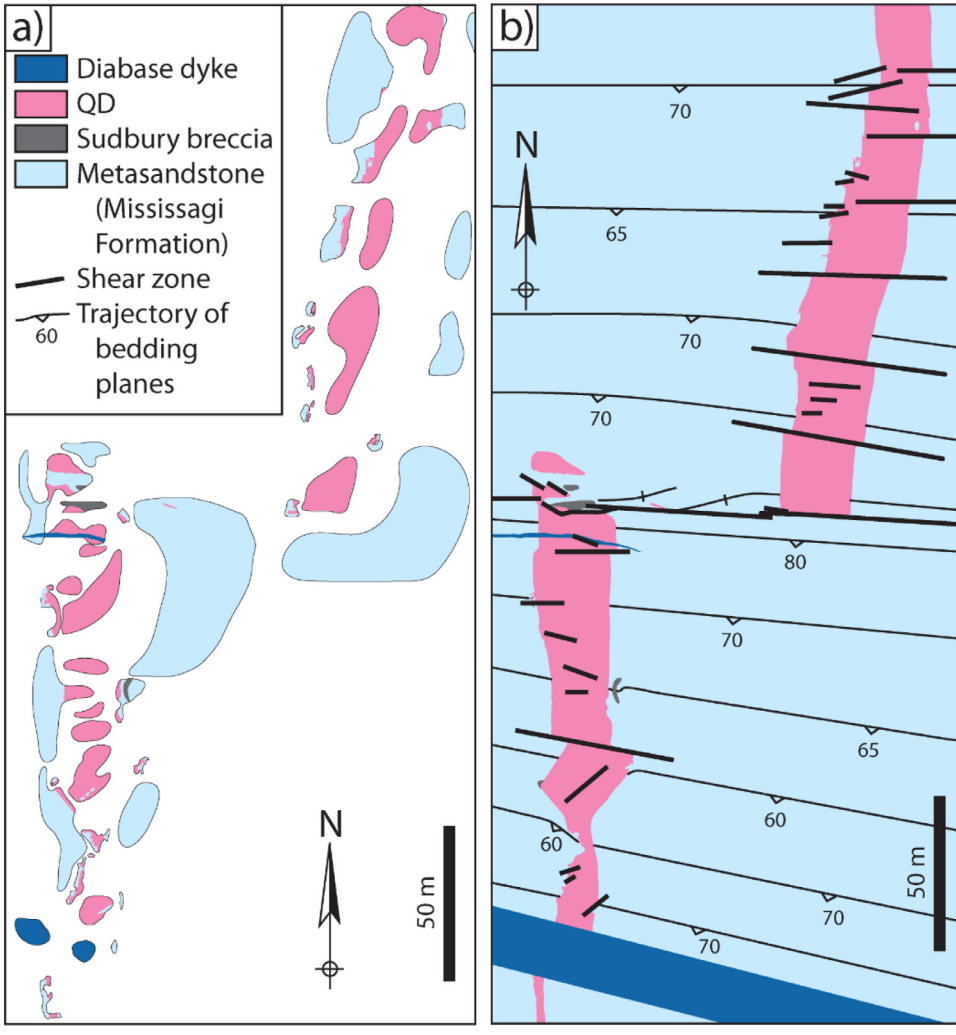

Fig. 33. Geological map of the Southern outcrop; a) Map displaying the outcrops visited in the field; b) Geological map of the CCO dyke.

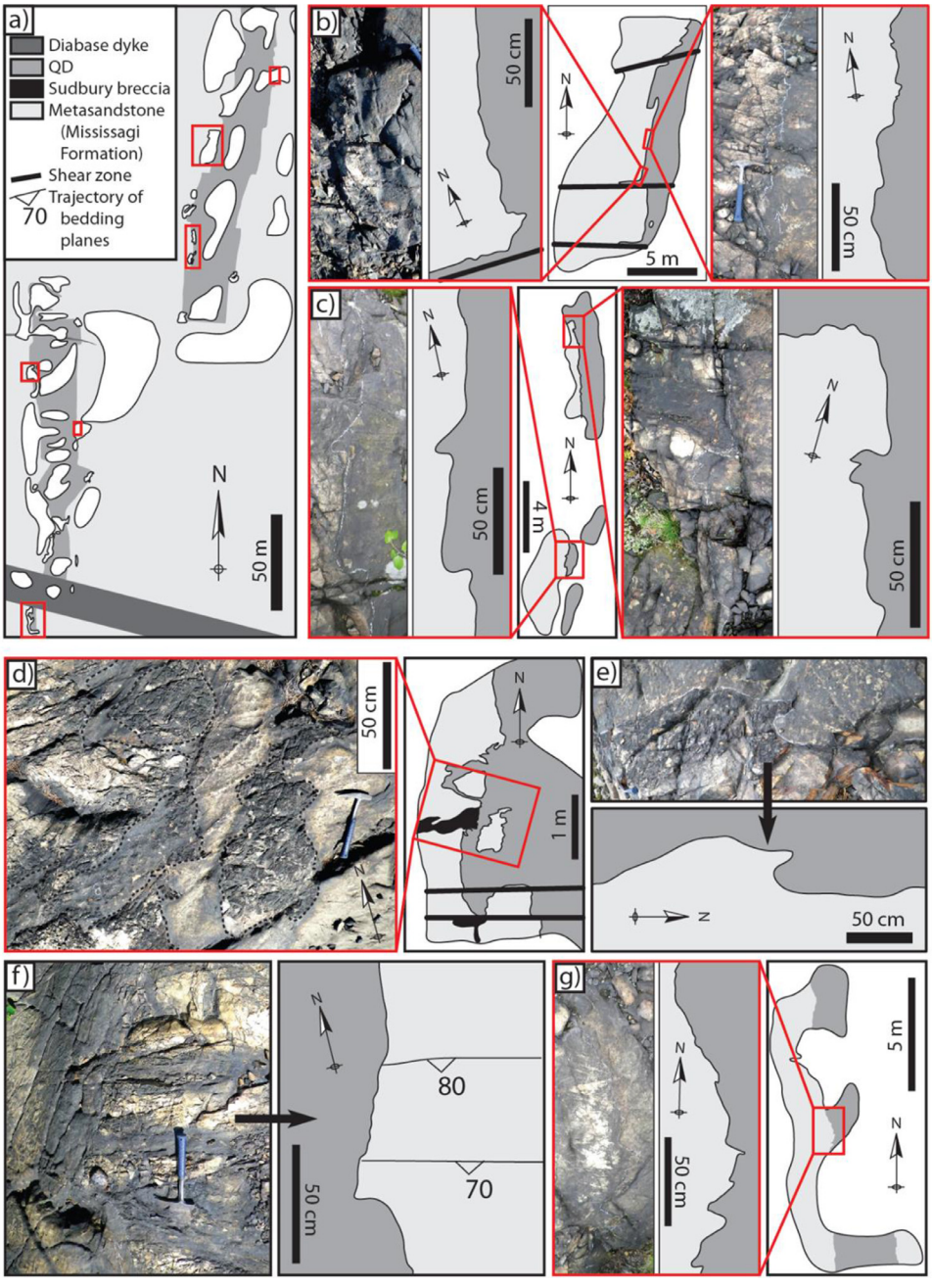

Fig. 34. Outcrop photographs and sketches of the margin of the CCO dyke, displaying contact relationships between the CCO dyke and metasandstone rocks.

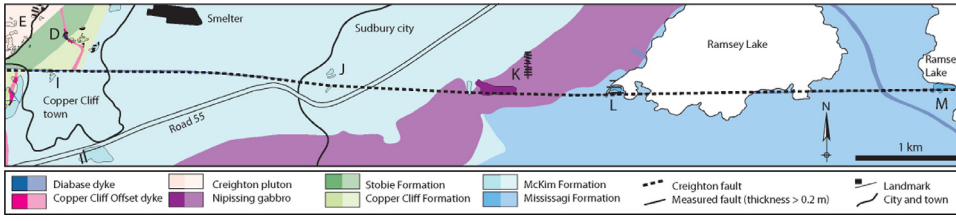

Fig. 35. Geological map displaying the outcrops of the Creighton fault (geology after [1] and outcrop location after [2]).

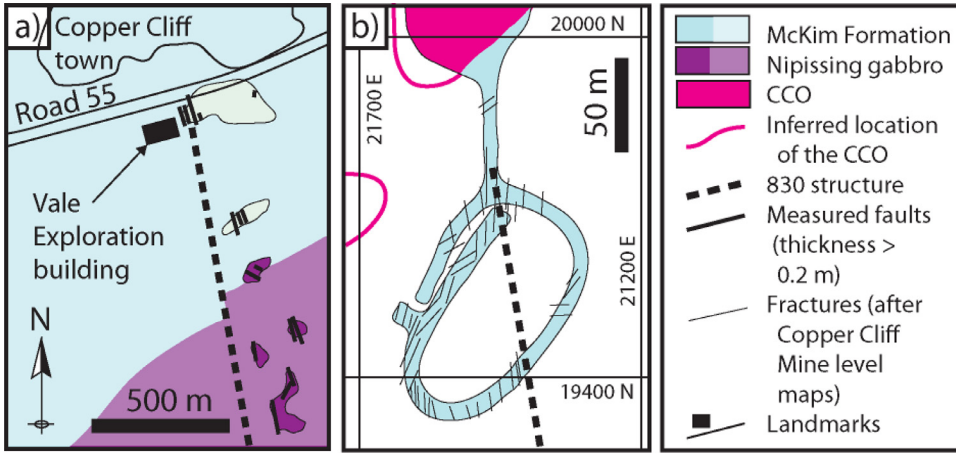

Fig. 36. Geological map of the 830 structure (shear zone); a) Surface outcrops near the Vale Exploration building; b) Geological map of the 3500 to 3350 levels (Copper Cliff Mine level plans).

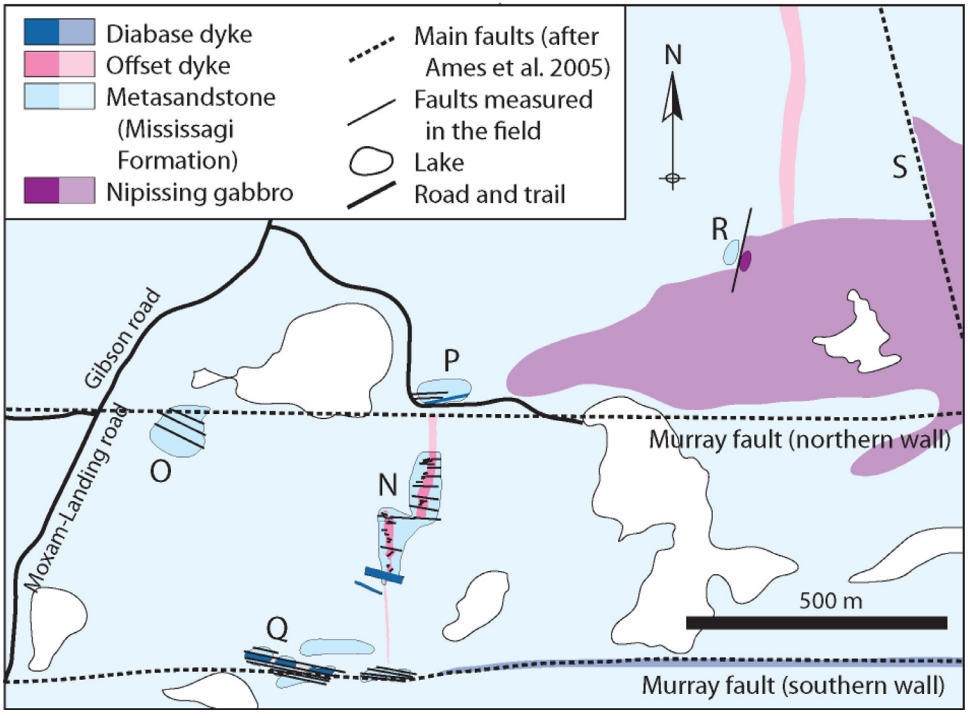

Fig. 37. Geological map displaying the Murray fault zone (area N corresponds to the Southern outcrop).

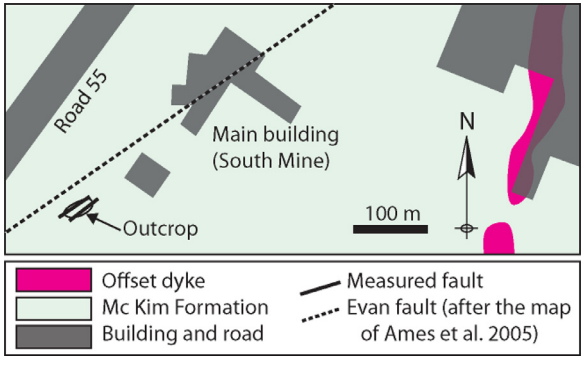

Fig. 38. Geological map displaying the Evan fault in the South Mine area.

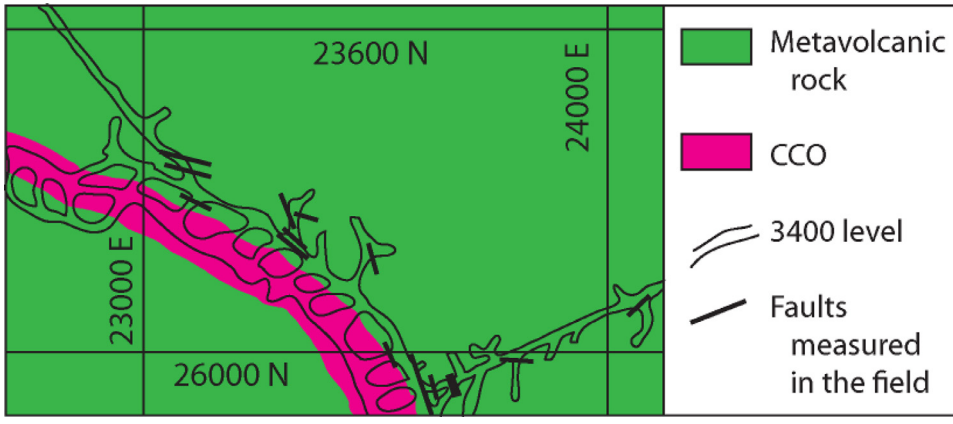

Fig. 39. Geological map of the 3400 level, displaying the faults measured in the field.

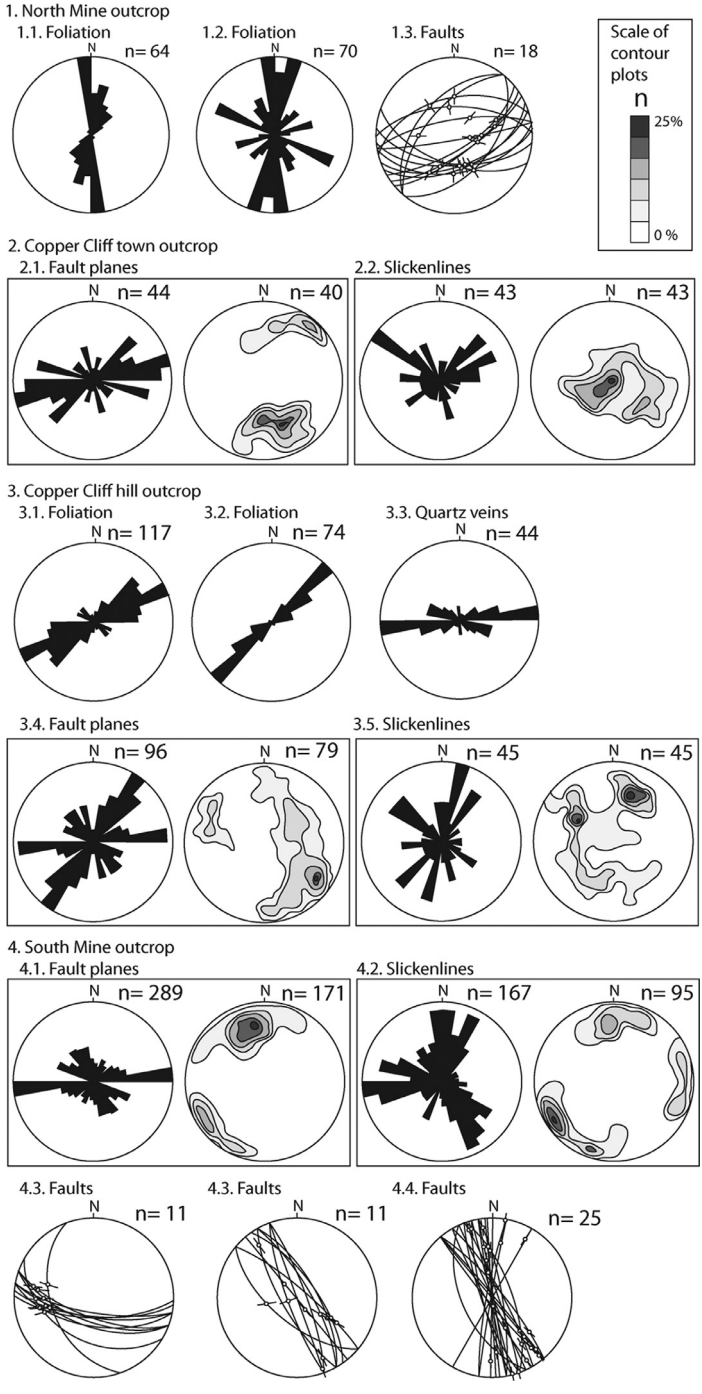

Fig. 40 (suite). Stereonet plots, Angelier and Rose diagrams (structures measured on CCO dyke outcrops; areas 1 to 5 on Fig. 15).

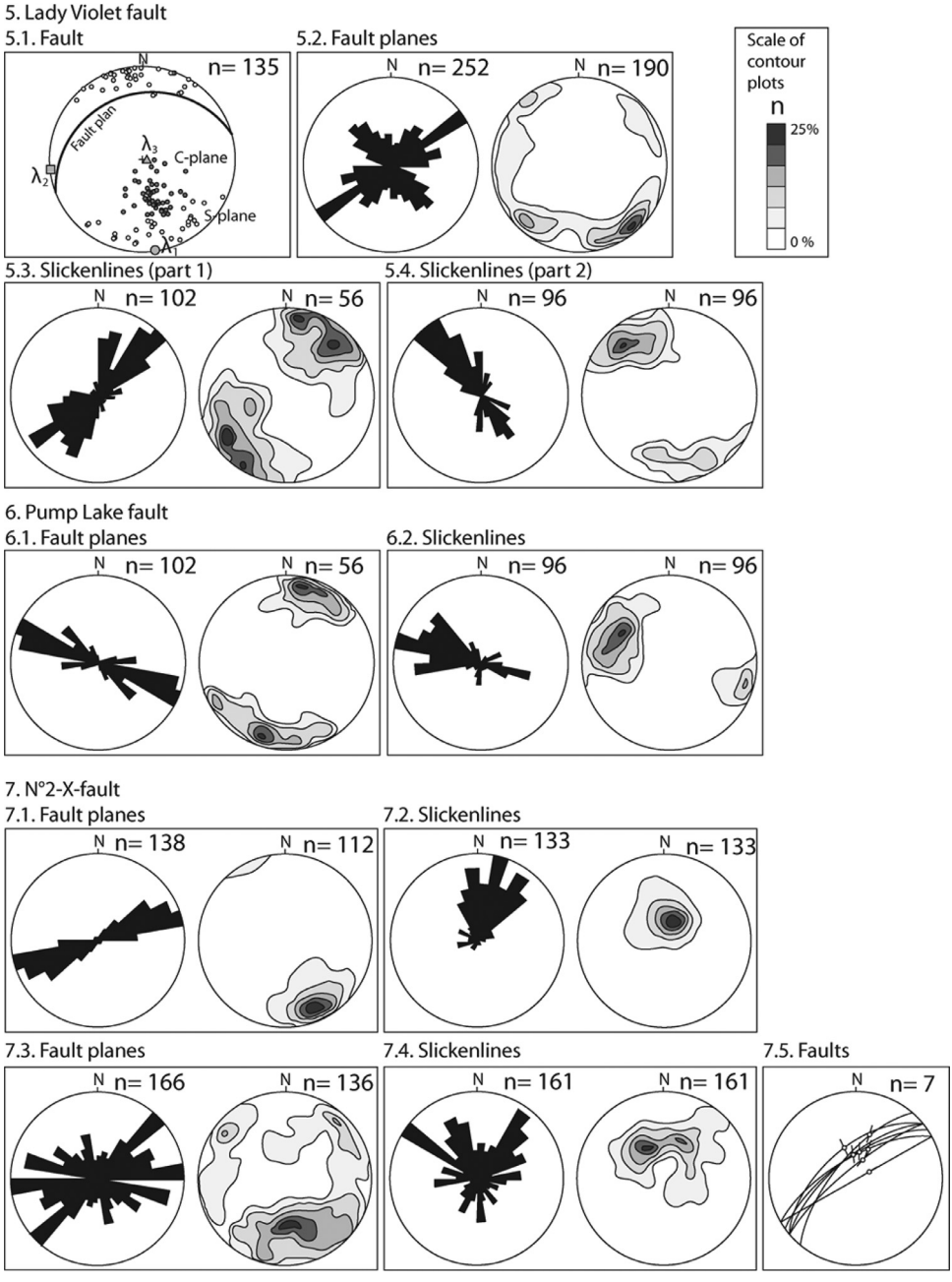

Fig. 40 (suite). Continued

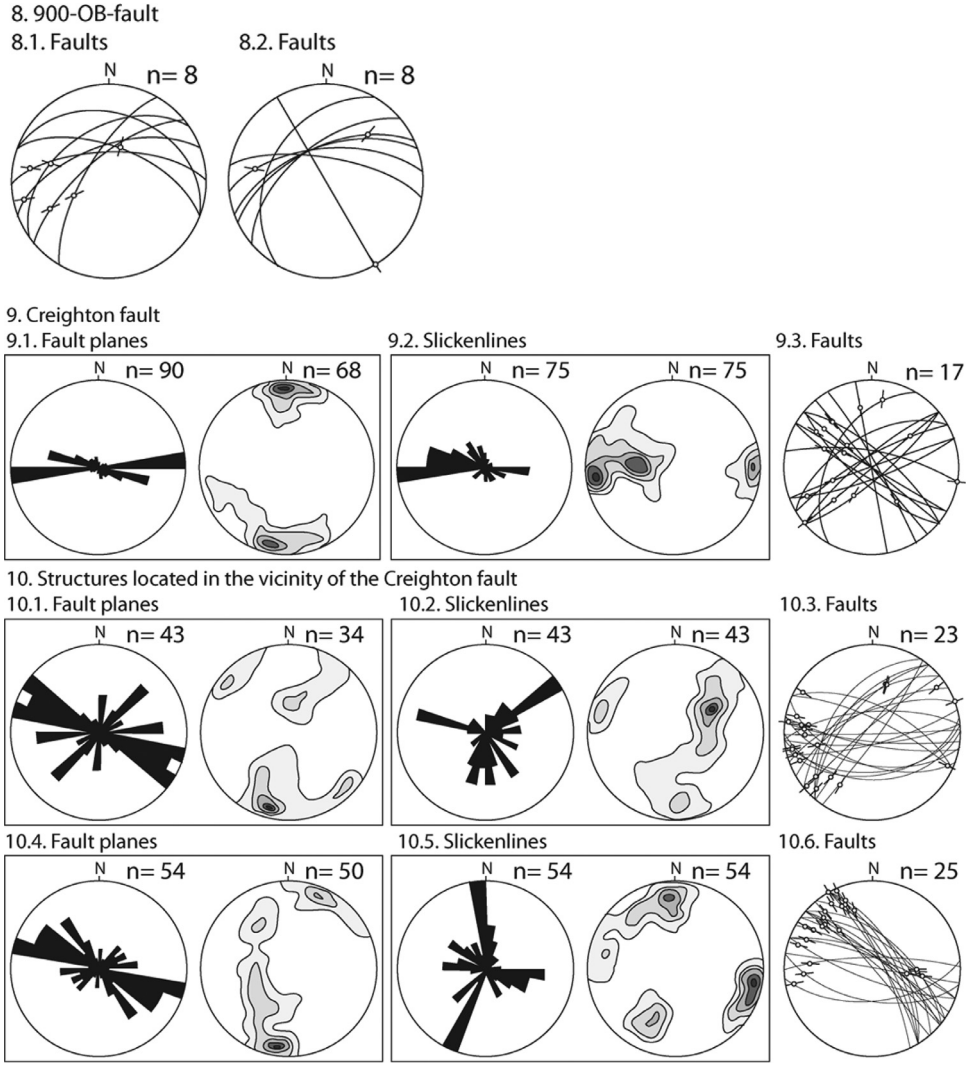

Fig. 40 (suite). Continued

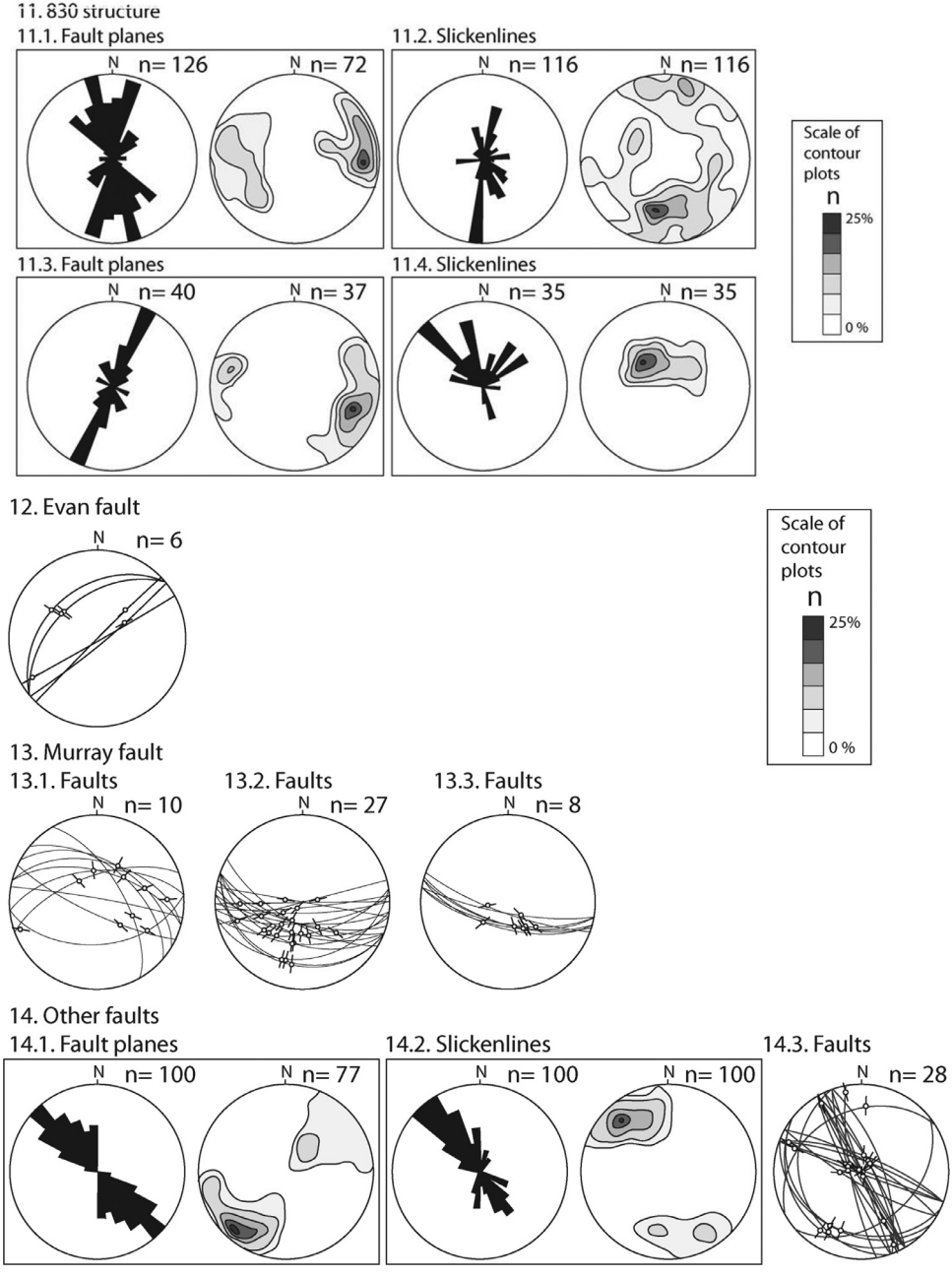

Fig. 40 (suite). Continued

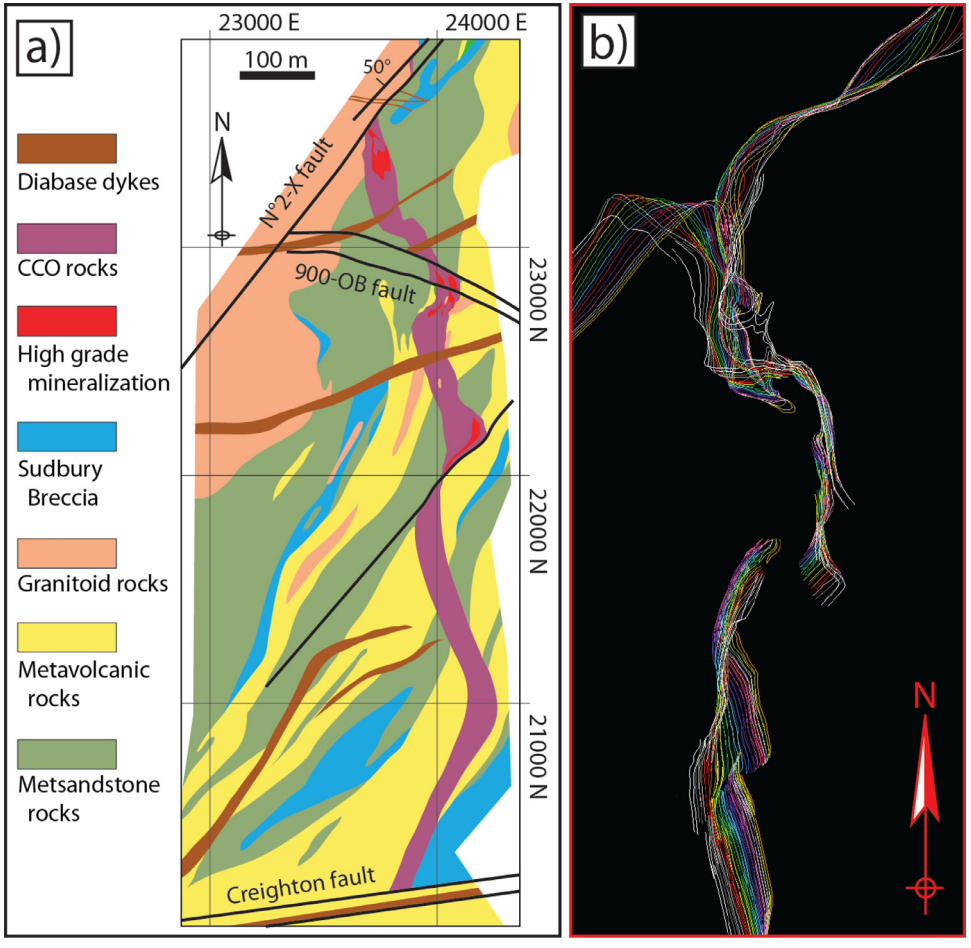

Fig. 41. Data used to compute the Move model; a) Copper Cliff Mine map of the 2000 level digitized using the Illustrator software (coordinate system in feet); b) Curves drawn from 19 simplified level maps using the Move software.

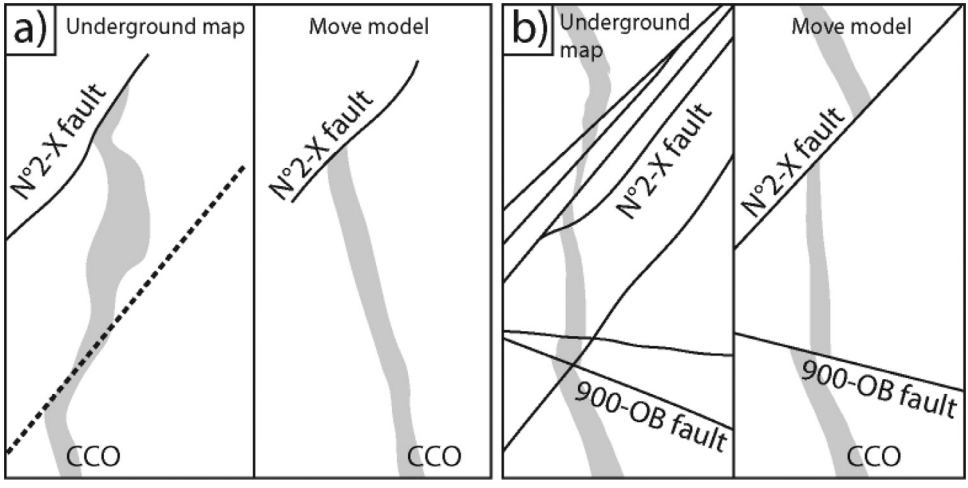

Fig. 42. The 800 (a) and 4000 (c) level maps of the N°2-X and 900-OB faults, and the simplified maps of the 800 (b) and 4000 (d) levels used to create the fault surfaces of the 3D models.

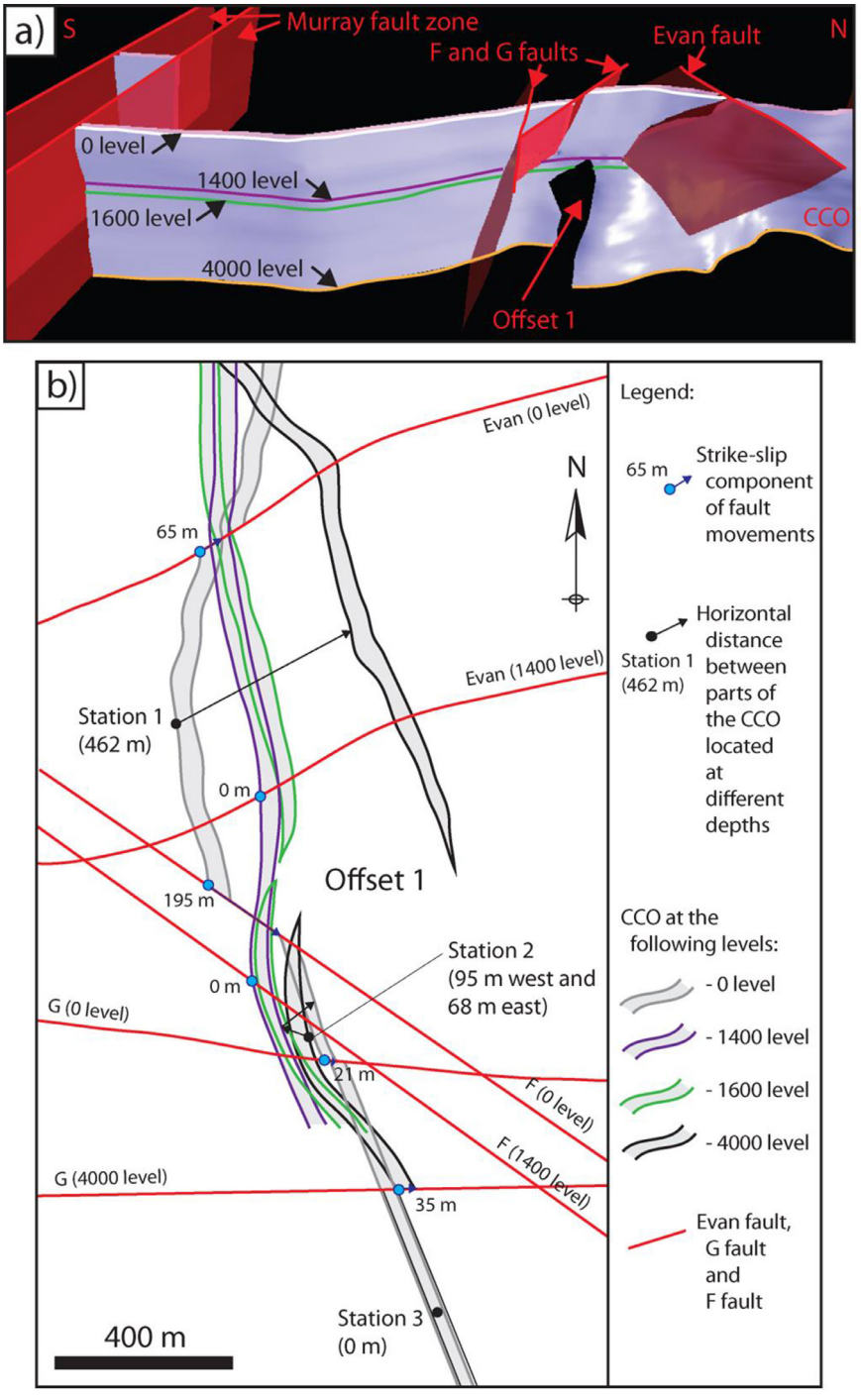

Fig. 43. Southern part of the CCO dyke; a) perspective view of the Move model; b) Horizontal sections of the Move model at levels 0, 1400, 1600 and 4000, which correspond, respectively, to the elevations 250 m, -177 m, -237 m and -970 m.

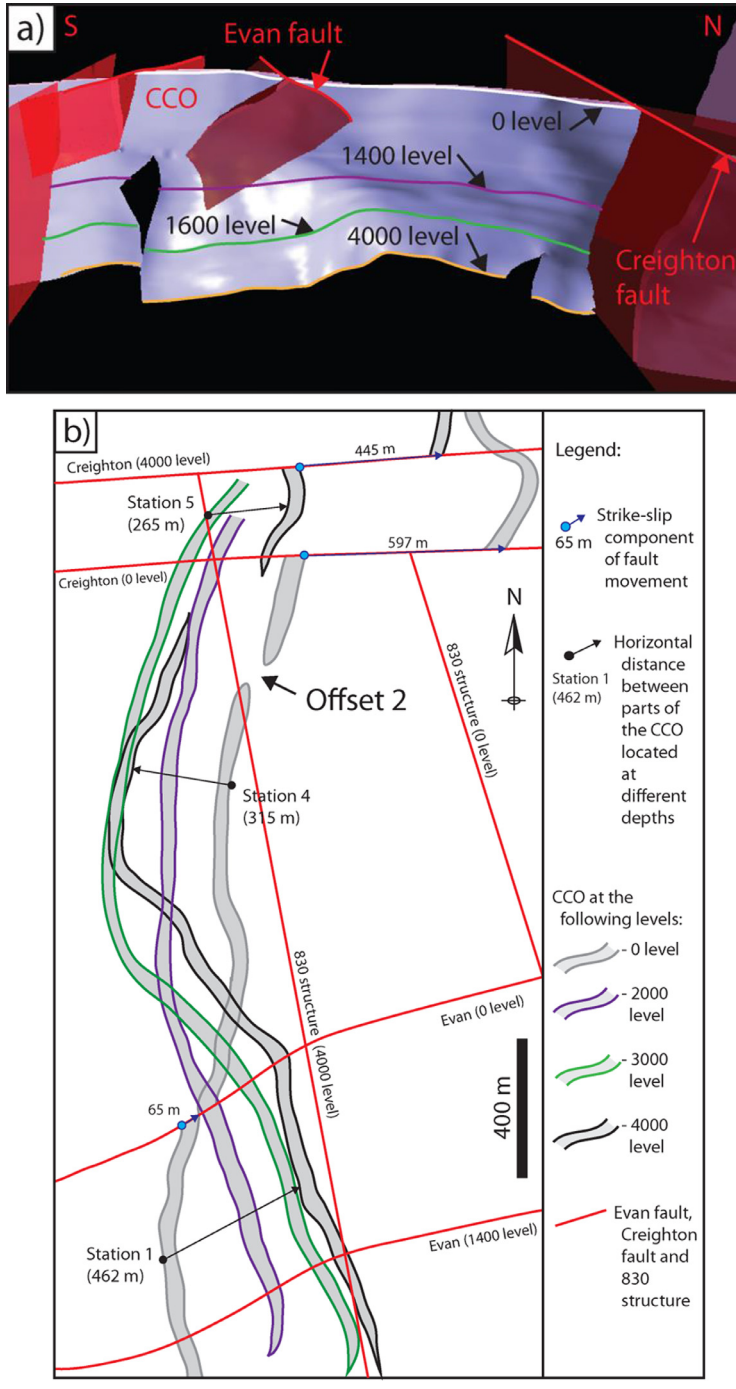

Fig. 44. CCO dyke in the 830 structure (shear zone) area; a) perspective view of the Move model; b) Horizontal sections of the Move model at levels 0, 2000, 3000 and 4000, which correspond, respectively, to the elevations 250 m, -360 m, -664 m and -970 m.

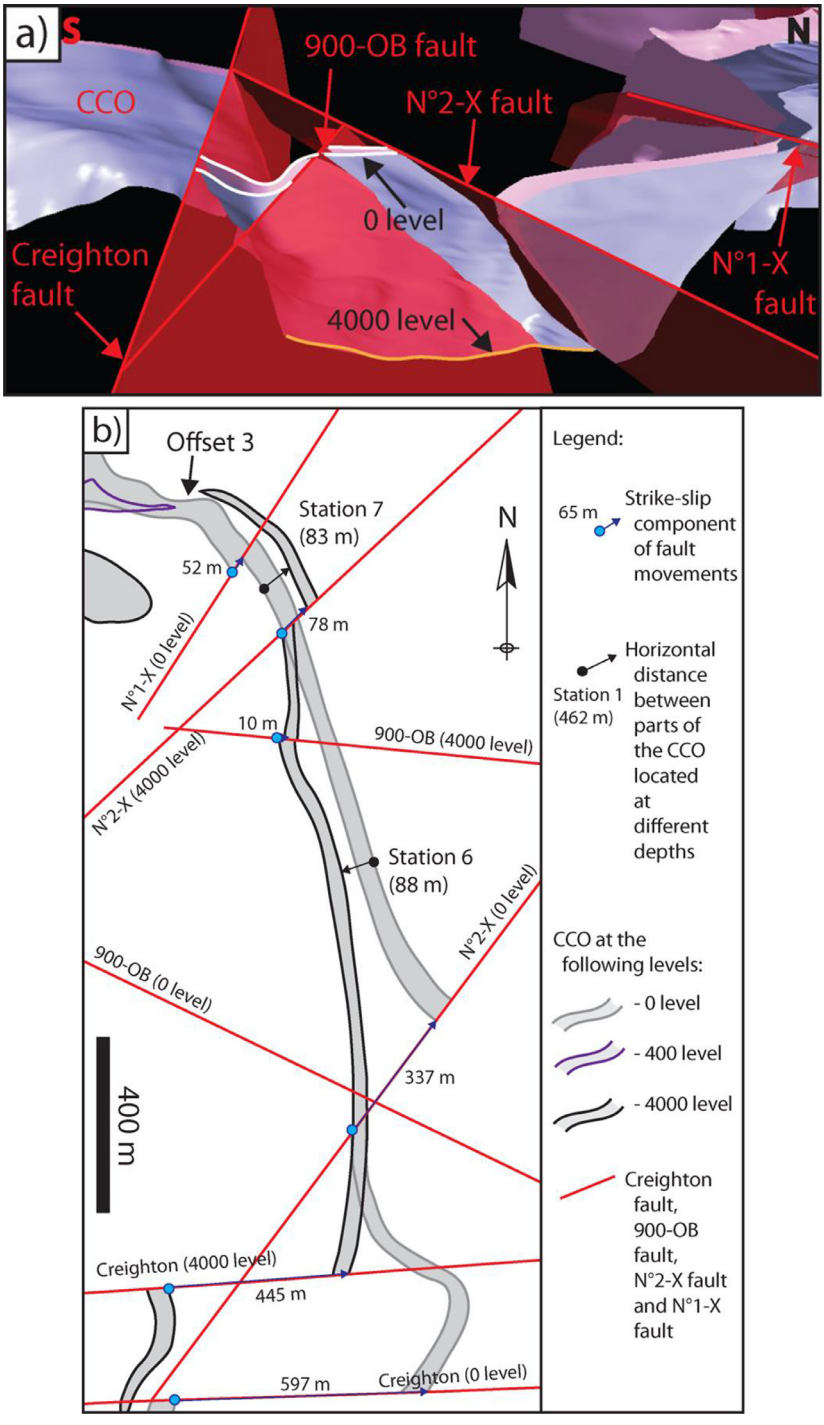

Fig. 45. Northern part of the CCO dyke; a) Perspective view of the Move model; b) Horizontal sections of the Move model at levels 0, 400 and 4000, which correspond, respectively, to the elevations 250 m, 128 m and -970 m

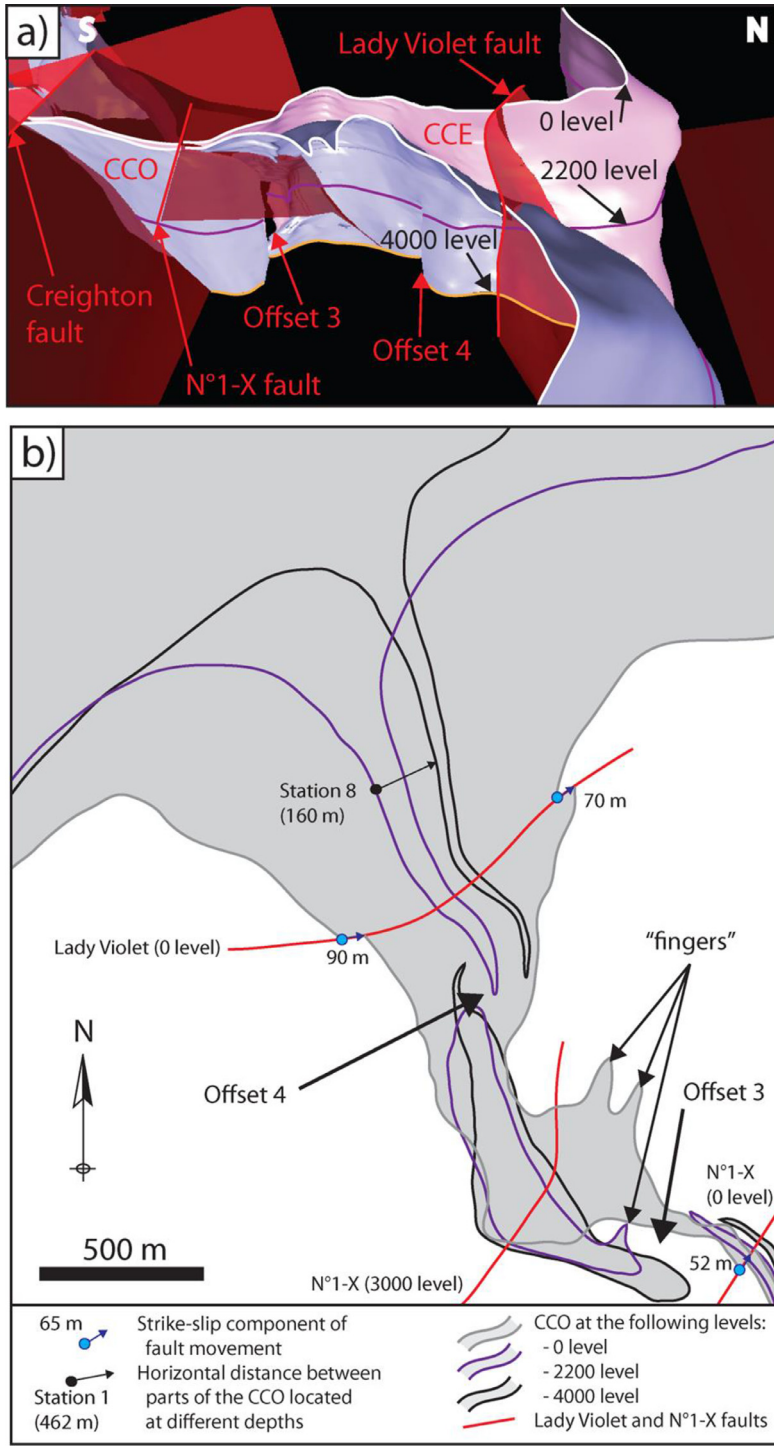

Fig. 46. CCE and underlying CCO dyke; a) Perspective view of the Move model; b) Horizontal sections of the Move model at levels 0, 2200 and 4000, which correspond, respectively, to the elevations 250 m, -420 m and -970 m.

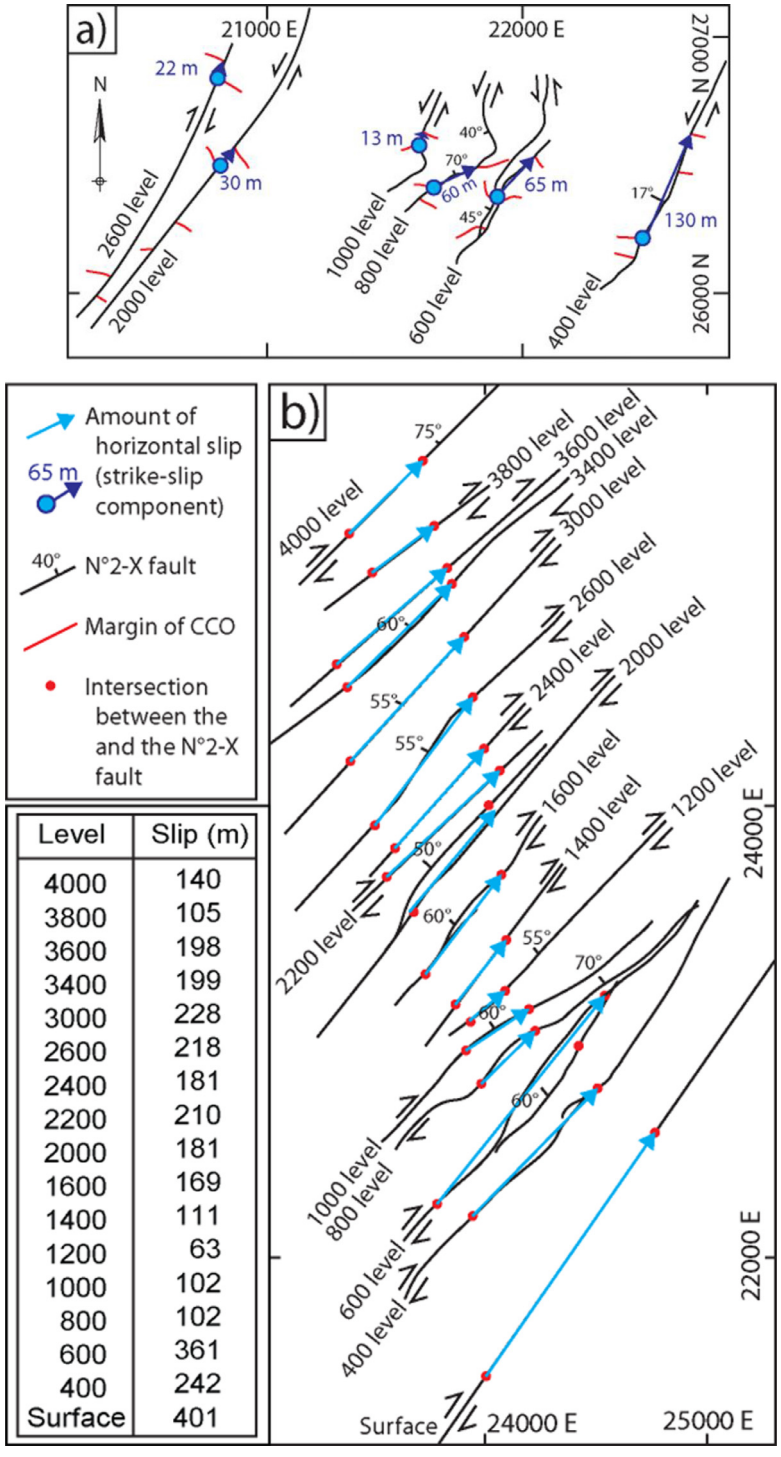

Level	Slip (m)
4000	140
3800	105
3600	198
3400	199
3000	228
2600	218
2400	181
2200	210
2000	181
1600	169
1400	111
1200	63
1000	102
800	102
600	361
400	242
Surface	401

Fig. 47. Maps of the traces of the N°1-X (a) and N°2-X fault planes, from surface to the 4000 levels. These maps display the post-cratering horizontal strike-slip components of the faults.

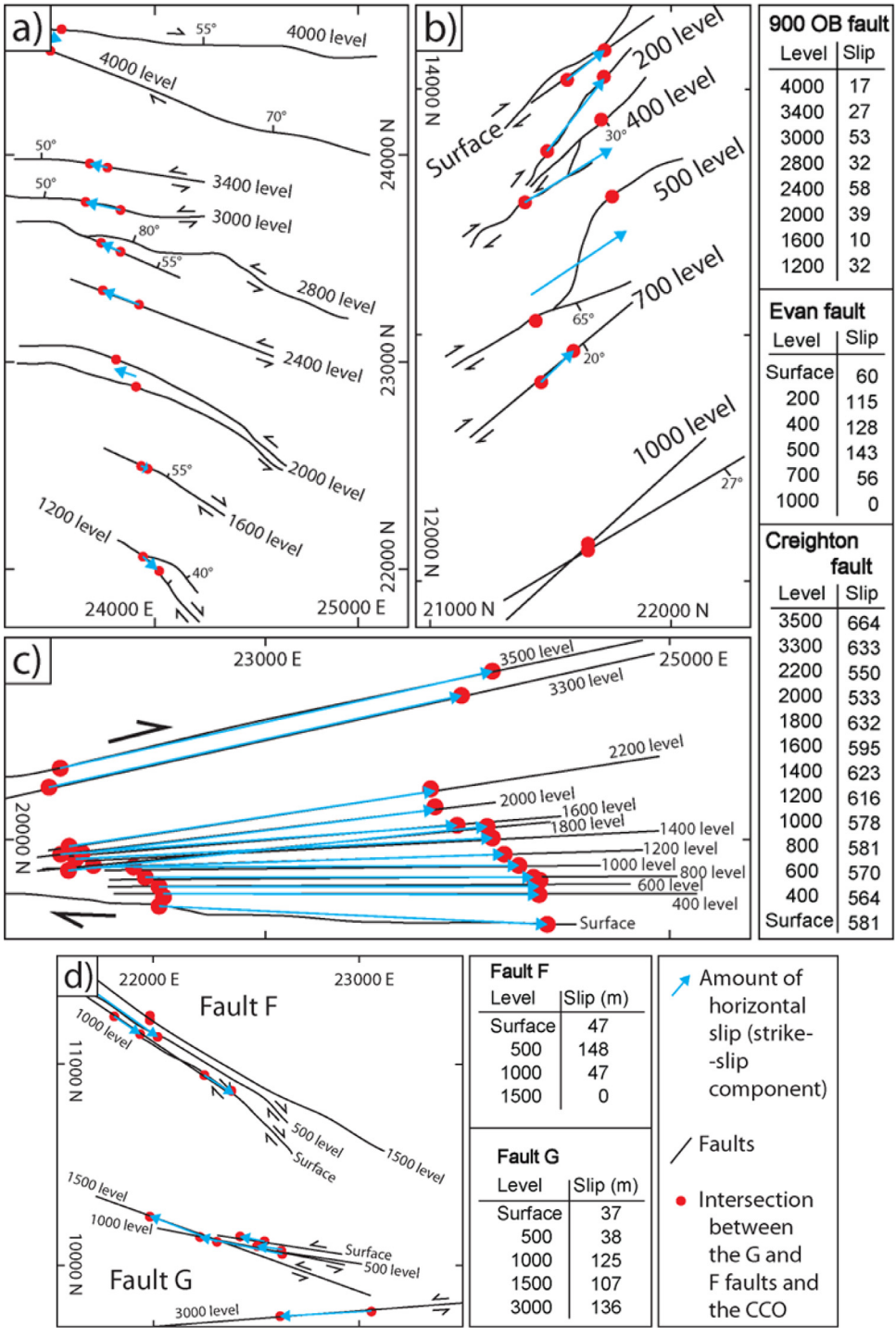

900 OB fault

Level	Slip
4000	17
3400	27
3000	53
2800	32
2400	58
2000	39
1600	10
1200	32

Evan fault

Level	Slip
Surface	60
200	115
400	128
500	143
700	56
1000	0

Creighton fault

Level	Slip
3500	664
3300	633
2200	550
2000	533
1800	632
1600	595
1400	623
1200	616
1000	578
800	581
600	570
400	564
Surface	581

Fault F

Level	Slip (m)
Surface	47
500	148
1000	47
1500	0

Fault G

Level	Slip (m)
Surface	37
500	38
1000	125
1500	107
3000	136

Amount of horizontal slip (strike--slip component)

Faults

Intersection between the G and F faults and the CCO

Fig. 48. Maps of the traces of the 900-OB (a), Evan (b), Creighton (c), F and G (d) fault planes, from surface to the 4000 levels. These maps display the post-cratering horizontal strike-slip components of the faults.

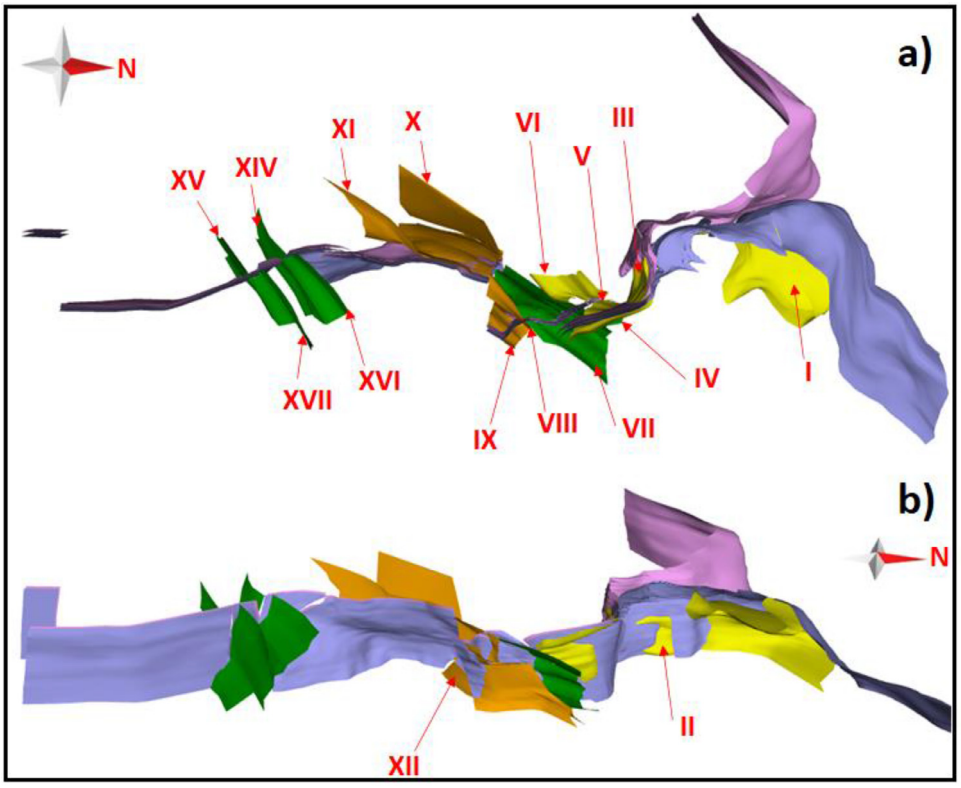

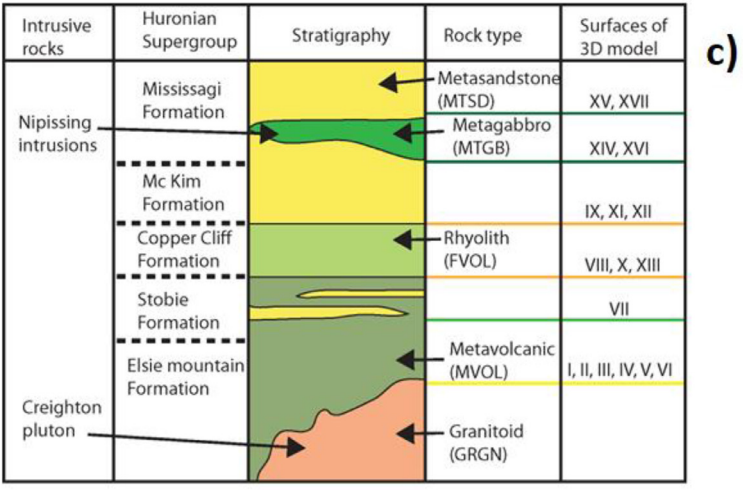

Fig. 49. (a) Perspective views of the Move model displaying the CCO dyke, the CCE, the fault planes and the I to XVII surfaces, which correspond to lithological contacts; (b) Simplified stratigraphic column displaying pre-impact lithologies, as well as surfaces I to XVII of the Move model.

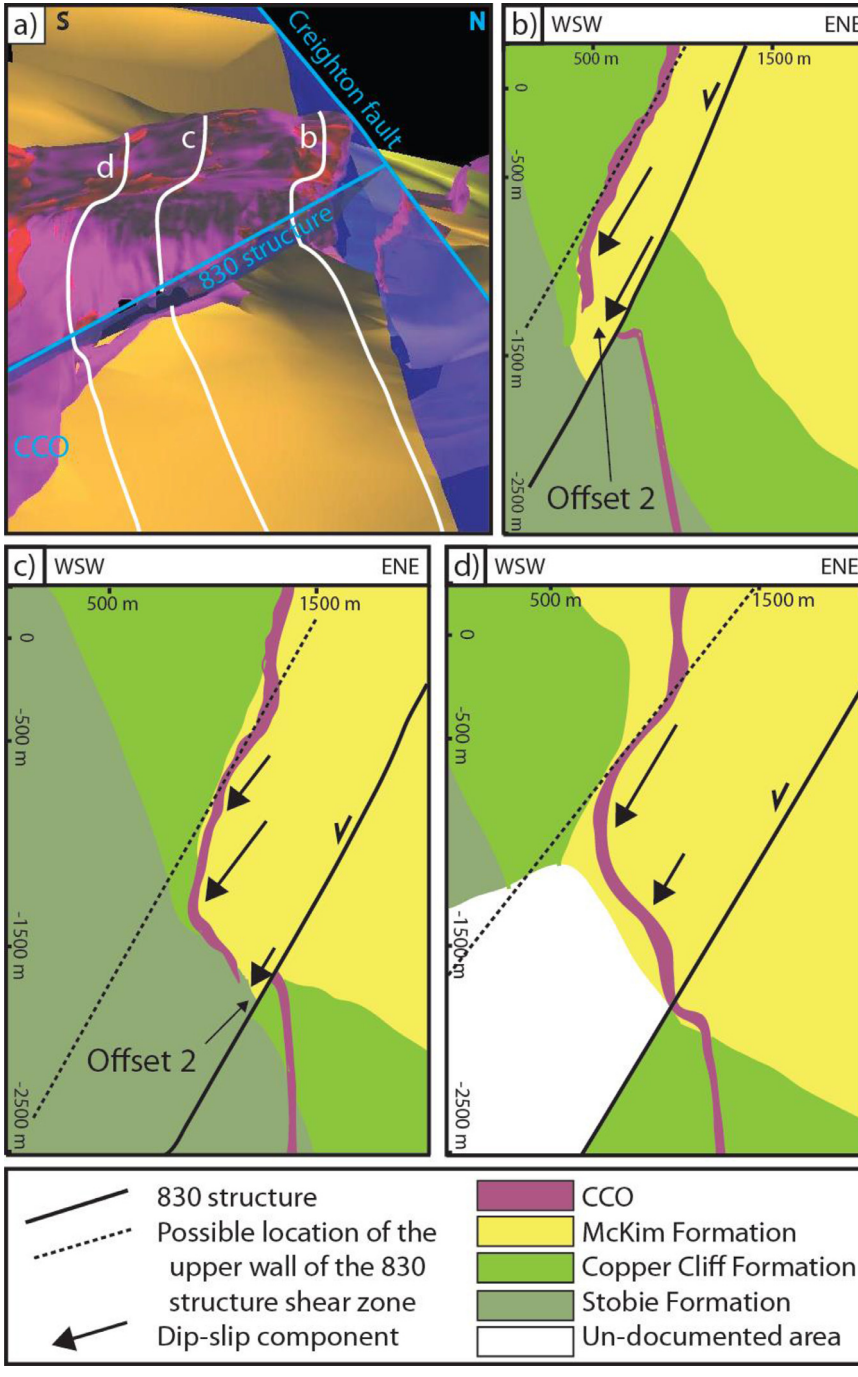

Fig. 50. Perspective view (a) and vertical sections (b, c, d) of the Datamine model, displaying the 830 shear zone, the CCO dyke and pre-impact rocks.

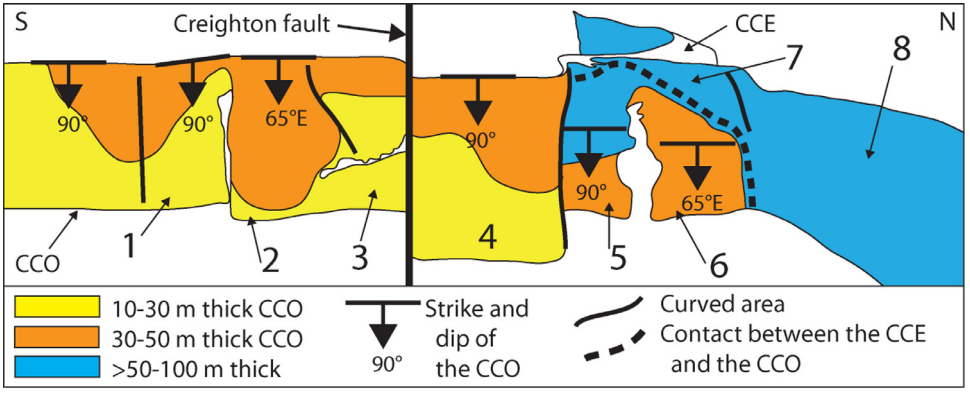

Fig. 51. Sketch of the orientation and thickness of the CCE and CCO dyke. Note that the boundary between the < and > 30 m thick parts of the CCO dyke is arbitrarily located, as thickness variation is progressive in the CCO dyke.

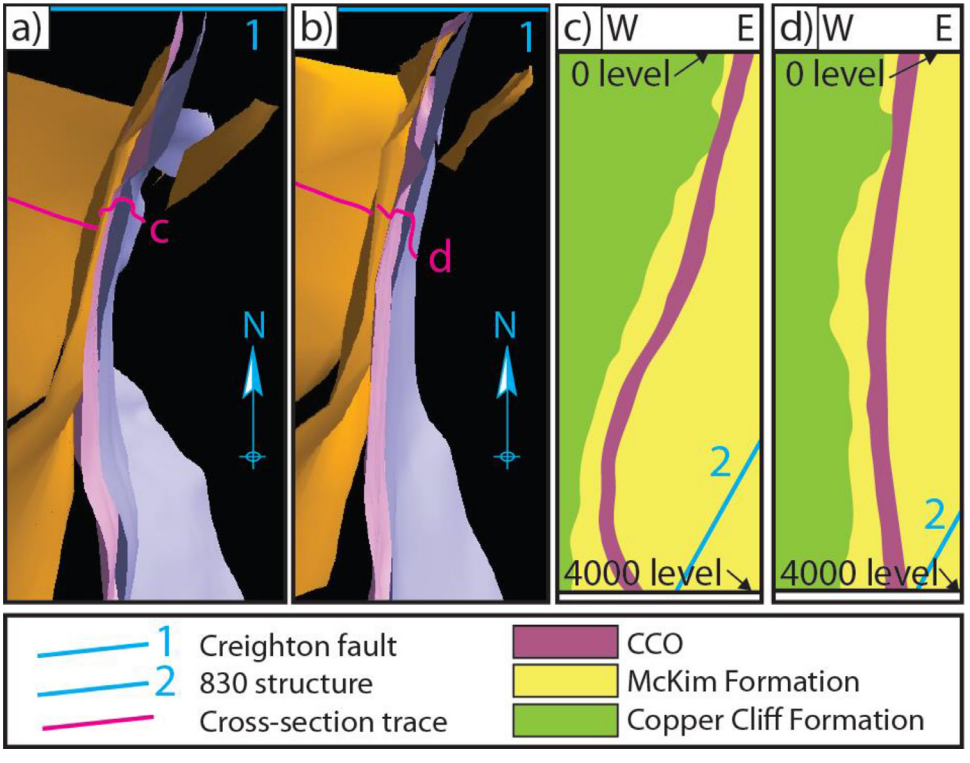

Fig. 52. Perspective views (a, b) and vertical sections (c, d) of the un-restored (a, c) and restored (b, d) Move models. Offset 2 is not displayed because the Move model runs only to the -970 m elevation, while Offset 2 is located at deeper elevations.

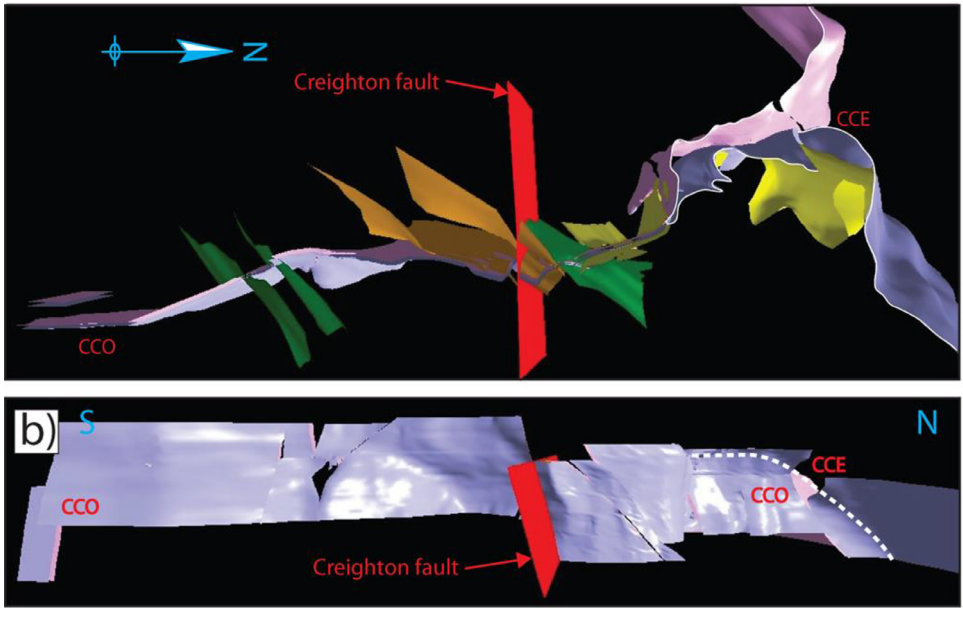

Fig. 53. Top view (a) and perspective view (b) of the "un-faulted" Move model.

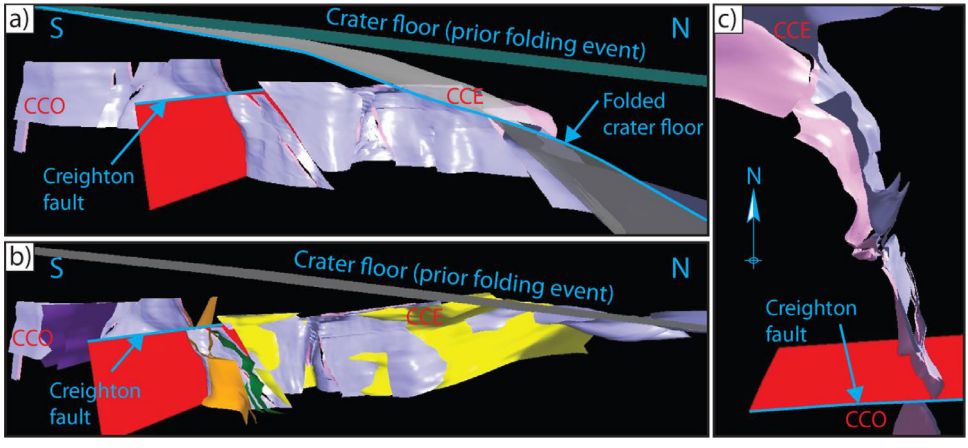

Fig. 54. Perspective views of the "un-faulted" (a) and "un-folded" (b, c) Move model.

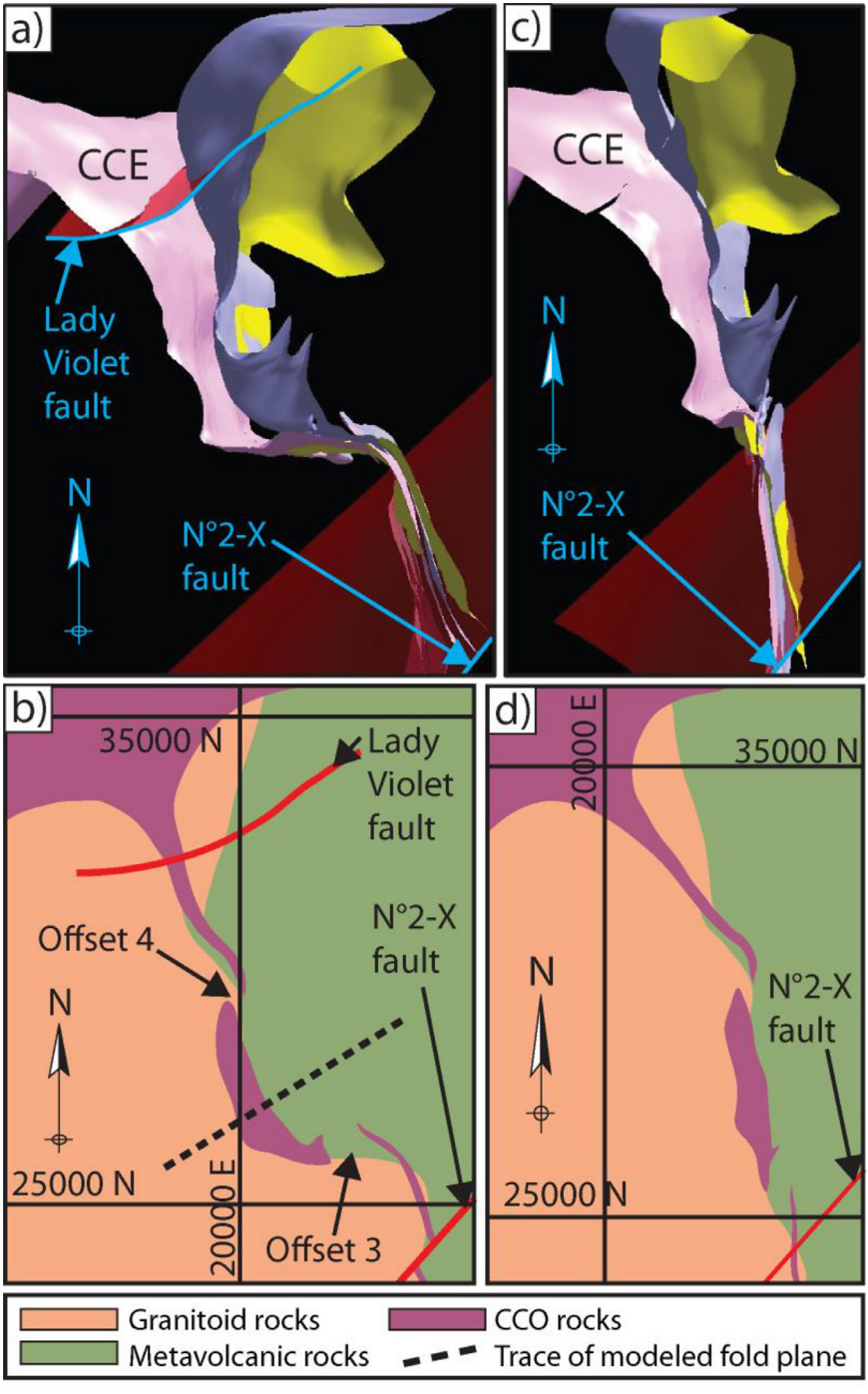

Fig. 55. Perspective views (a, c) and horizontal sections of the -450 elevation (b, d) of the un-restored (a, b) and restored (c, d) Move models.

Ethics Statement

The authors, Lucie Mathieu, Ulrich Riller, Lisa Gibson and Peter Lightfoot, declare no conflict of interest.

Data Availability

Tables 1, 2, 3 and 4 are available as a .xlsx file. These tables report structural data measured in the field. These tables can be accessed through the data repository Mendeley Data [4].

CRediT Author Statement

Lucie Mathieu: Conceptualization, Methodology, Software, Writing original draft, Visualization, Investigation; **Ulrich Riller:** Conceptualization, Funding acquisition, Validation, Writing review & editing; **Lisa Gibson:** Validation, Writing review & editing; **Peter Lightfoot:** Validation, Writing review & editing.

Declaration of Competing Interest

The study as was carried in collaboration with and supported by Vale, Copper Cliff, as well as the Center of Excellence for Mining Innovation, Sudbury, under RA 1353-CA-030.

Acknowledgments

Thanks are addressed to the geologists of the Copper Cliff Mine and to McMaster University field assistants, namely Gordon Bailey, James McDonald, Joseph d'Olivera, Kristen Simpson and Peter Stewart.

References

[1] D.E. Ames, A. Davidson, J.L. Buckle, K.D. Card, Geology, Sudbury Bedrock Compilation, Ontario, 4570, 2005 Geol. Surv. Canada, Open File.
[2] L.B. Cochrane, The Creighton Fault: Location Description, Calculation of Movement, Regional Setting and Possible Mechanisms of Formation, 1983 Report prepared for Science North.
[3] P. Launeau, P.-Y. Robin, Fabric analysis using the intercept method, Tectonophysics 267 (1996) 91–119.
[4] L. Mathieu, Copper_Cliff_Offset_dyke, Mendeley Data. V1, 2021, doi:10.17632/hfzs627ps3.1.